LETTER

doi:10.1038/nature25188

Paternal chromosome loss and metabolic crisis contribute to hybrid inviability in *Xenopus*

Romain Gibeaux[1], Rachael Acker[1], Maiko Kitaoka[1], Georgios Georgiou[2], Ila van Kruijsbergen[2], Breanna Ford[3], Edward M. Marcotte[4], Daniel K. Nomura[3], Taejoon Kwon[5], Gert Jan C. Veenstra[2] & Rebecca Heald[1]

Hybridization of eggs and sperm from closely related species can give rise to genetic diversity, or can lead to embryo inviability owing to incompatibility. Although central to evolution, the cellular and molecular mechanisms underlying post-zygotic barriers that drive reproductive isolation and speciation remain largely unknown[1,2]. Species of the African clawed frog *Xenopus* provide an ideal system to study hybridization and genome evolution. *Xenopus laevis* is an allotetraploid with 36 chromosomes that arose through interspecific hybridization of diploid progenitors, whereas *Xenopus tropicalis* is a diploid with 20 chromosomes that diverged from a common ancestor approximately 48 million years ago[3]. Differences in genome size between the two species are accompanied by organism size differences, and size scaling of the egg and subcellular structures such as nuclei and spindles formed in egg extracts[4]. Nevertheless, early development transcriptional programs, gene expression patterns, and protein sequences are generally conserved[5,6]. Whereas the hybrid produced when *X. laevis* eggs are fertilized by *X. tropicalis* sperm is viable, the reverse hybrid dies before gastrulation[7,8]. Here we apply cell biological tools and high-throughput methods to study the mechanisms underlying hybrid inviability. We reveal that two specific *X. laevis* chromosomes are incompatible with the *X. tropicalis* cytoplasm and are mis-segregated during mitosis, leading to unbalanced gene expression at the maternal to zygotic transition, followed by cell-autonomous catastrophic embryo death. These results reveal a cellular mechanism underlying hybrid incompatibility that is driven by genome evolution and contributes to the process by which biological populations become distinct species.

Hybrids produced through fertilization of *X. laevis* eggs with *X. tropicalis* sperm ($l_e \times t_s$) are viable, whereas *X. tropicalis* eggs fertilized by *X. laevis* sperm ($t_e \times l_s$) are not (Fig. 1a)[7,8]. Although cleavage divisions and rate of development of $t_e \times l_s$ hybrids were initially similar to *X. tropicalis* ($t_e \times t_s$) (Fig. 1b), hybrid embryos died abruptly as late blastulae and never initiated gastrulation. Before their death, hybrid embryos took on a deformed mushroom-like shape before lysing from the vegetal pole (Fig. 1c and Supplementary Video 1). Explants prepared from the opposite pole (animal caps) of mid-blastula $t_e \times l_s$ embryos also died within a few hours, indicating that embryo death is cell autonomous and not a result of faulty developmental cues (Fig. 1d and Supplementary Video 2). In contrast to $t_e \times l_s$ hybrids that die as embryos, haploid *Xenopus* embryos develop to the tadpole stage[8,9], suggesting that hybrid death is due to factors brought in by the *X. laevis* sperm to the *X. tropicalis* egg during fertilization. Irradiation of *X. laevis* sperm before fertilization, which destroys the DNA[10,11], resulted in a haploid phenotype (Fig. 1e and Supplementary Videos 3 and 4), indicating that $t_e \times l_s$ embryo death is due to the presence of the *X. laevis* genome. Cybrid embryos generated by irradiating *X. tropicalis* eggs, destroying the maternal DNA[8] before fertilization with *X. laevis* sperm, died before gastrulation similar to $t_e \times l_s$ embryos, indicating that hybrid inviability does not result from a conflict between the paternal and maternal genomes (Extended Data Table 1).

To visualize the dynamics of hybrid cell divisions, we injected mRNAs encoding fluorescent fusion proteins to label embryo chromosomes and mitotic spindles, and observed animal caps at early stage 9, which revealed anaphase defects and chromosome mis-segregation (Fig. 1f and Supplementary Video 5). Immunofluorescence of whole embryos confirmed the presence of lagging chromosomes and chromosome bridges in cells throughout hybrid blastulae, as well as the formation of micronuclei in interphase, whereas no such defects were observed in *X. tropicalis* embryos (Fig. 1g) or in the reverse viable hybrid (data not shown). Imaging of $t_e \times l_s$ embryos from stage 4 (eight cells) to stage 9 (thousands of cells) revealed micronuclei in 6–10% of the cells throughout hybrid development, but not in the *X. tropicalis* control (Extended Data Fig. 1a, b), indicating that chromosome mis-segregation in $t_e \times l_s$ hybrid embryos is unrelated to changes in gene expression at the onset of zygotic genome activation. Because the regular ploidy supported by the *X. tropicalis* egg is $N = 20$ chromosomes, but the $t_e \times l_s$ hybrid zygote must accommodate 28 chromosomes, we tested whether an increase in ploidy was causing chromosome mis-segregation and embryo death by applying a cold shock to *X. tropicalis* zygotes a few minutes after fertilization to suppress polar body extrusion and increase their ploidy to $N = 30$ chromosomes (Extended Data Fig. 1c). Micronuclei were not observed in cold-shocked embryos, which developed to the tailbud stage similarly to haploid embryos (Extended Data Fig. 1d). Thus, increasing the ploidy of *X. tropicalis* embryos does not cause chromosome mis-segregation or cell death, indicating a specific role for the *X. laevis* genome in hybrid inviability.

To determine whether assembly and function of the mitotic apparatus was affected, we used the *in vitro* egg extract system to examine spindle assembly and mitotic chromosome morphology. Metaphase-arrested *X. tropicalis* egg extract reconstituted spindle formation around nuclei isolated from stage 8 *X. tropicalis* ($N = 20$), *X. laevis* ($N = 36$), and viable hybrid embryos ($l_e \times t_s$; $N = 28$) (Fig. 2a). Spindle width scaled slightly with increasing genome size, but microtubule distribution was not affected by either genome size or content (Extended Data Fig. 1e), indicating that the presence of *X. laevis* DNA did not impair spindle assembly in *X. tropicalis* cytoplasm. To investigate chromosome morphology, *X. laevis* sperm nuclei were cycled through S phase in either *X. laevis* or *X. tropicalis* egg extract, induced to arrest in metaphase, and then stained with a DNA dye and antibodies to either CENP-A, the core centromeric histone variant, or Ndc80, an outer kinetochore component essential for linking centromeres to spindle microtubules[12]. Two fluorescent spots per chromosome were often visible in either extract, suggesting that the *X. tropicalis* extract is capable of replicating the *X. laevis* genome to generate duplicated

[1]Department of Molecular and Cell Biology, University of California, Berkeley, California 94720, USA. [2]Radboud University, Department of Molecular Developmental Biology, Faculty of Science, Radboud Institute for Molecular Life Sciences, 6500 HB Nijmegen, The Netherlands. [3]Departments of Chemistry and Nutritional Sciences and Toxicology, University of California, Berkeley, California 94720, USA. [4]Department of Molecular Bioscience, Center for Systems and Synthetic Biology, Institute for Cellular and Molecular Biology, The University of Texas at Austin, Austin, Texas 78712, USA. [5]Department of Biomedical Engineering, Ulsan National Institute of Science and Technology, Ulsan 44919, South Korea.

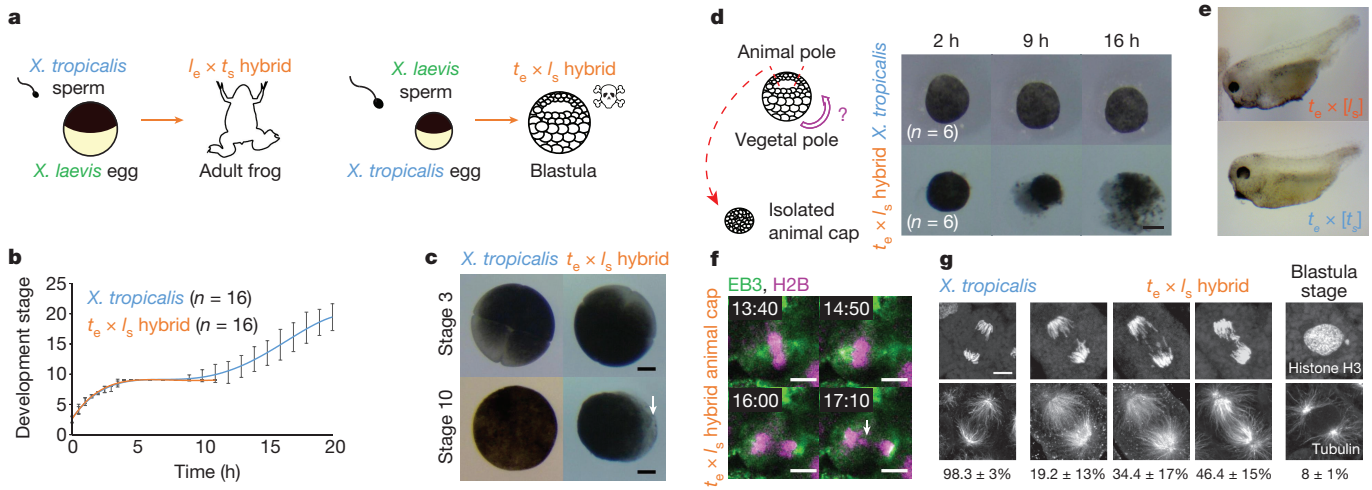

Figure 1 | Role of the *X. laevis* genome in $t_e \times l_s$ hybrid embryo death. **a**, Schematic of *X. laevis* and *X. tropicalis* cross-fertilization outcomes. **b**, Developmental timing in *X. tropicalis* and $t_e \times l_s$ hybrid embryos. Average is plotted for each time point. Error bars, s.d. **c**, Representative images of *X. tropicalis* and $t_e \times l_s$ hybrid embryos at stages 3 and 10 from experiments in **b** ($n = 16$ *X. tropicalis* and $n = 16$ $t_e \times l_s$ hybrid embryos from four independent experiments). Arrow indicates vegetal cells where death initiates. **d**, Schematic of animal cap assay and images of at 2, 9, and 16 h after isolation. Six animal caps were imaged and identical results were obtained in three different experiments. Scale bars in **c** and **d**, 200 μm. **e**, Images showing haploid phenotype following fertilization of *X. tropicalis* eggs with ultraviolet-irradiated sperm. Identical results were observed in $n = 3$ experiments. **f**, Time-lapse images of dividing cell in a $t_e \times l_s$ hybrid animal cap (Supplementary Video 5). Arrow indicates a mis-segregated chromosome. Mis-segregated chromosomes were observed in $n = 3$ live $t_e \times l_s$ hybrid animal caps in three experiments. Time is in minutes:seconds. **g**, Immunofluorescence images showing chromosome bridges, mis-segregated chromosomes, and micronuclei throughout $t_e \times l_s$ hybrid embryos. Scale bars in **f** and **g**, 10 μm. Quantification of $n = 81$ *X. tropicalis* and $n = 78$ $t_e \times l_s$ hybrid anaphases in $n = 17$ and 16 embryos, respectively, from four datasets obtained from three experiments presented as averages ± 1 s.d., show a significant difference by Fisher's 2×3 contingency test ($P = 0$). Quantification of micronuclei in $t_e \times l_s$ hybrid embryos is detailed in Extended Data Fig. 1b.

sister chromatids. However, we observed 13.5% fewer CENP-A-labelled and 12% fewer Ndc80-labelled chromosomes in *X. tropicalis* extract compared with *X. laevis* extract (Fig. 2b), suggesting that approximately two *X. laevis* chromosomes do not possess centromeres that become competent for kinetochore assembly following a cell cycle in *X. tropicalis* cytoplasm. Whole-genome sequencing of embryos at stage 9 before cell death revealed the specific loss of 228 megabases of *X. laevis* sequence from $t_e \times l_s$ hybrids (Fig. 2c), 96% of which was missing from just two chromosomes, 3L and 4L. By contrast, no genomic deletions were detected in viable $l_e \times t_s$ hybrid embryos

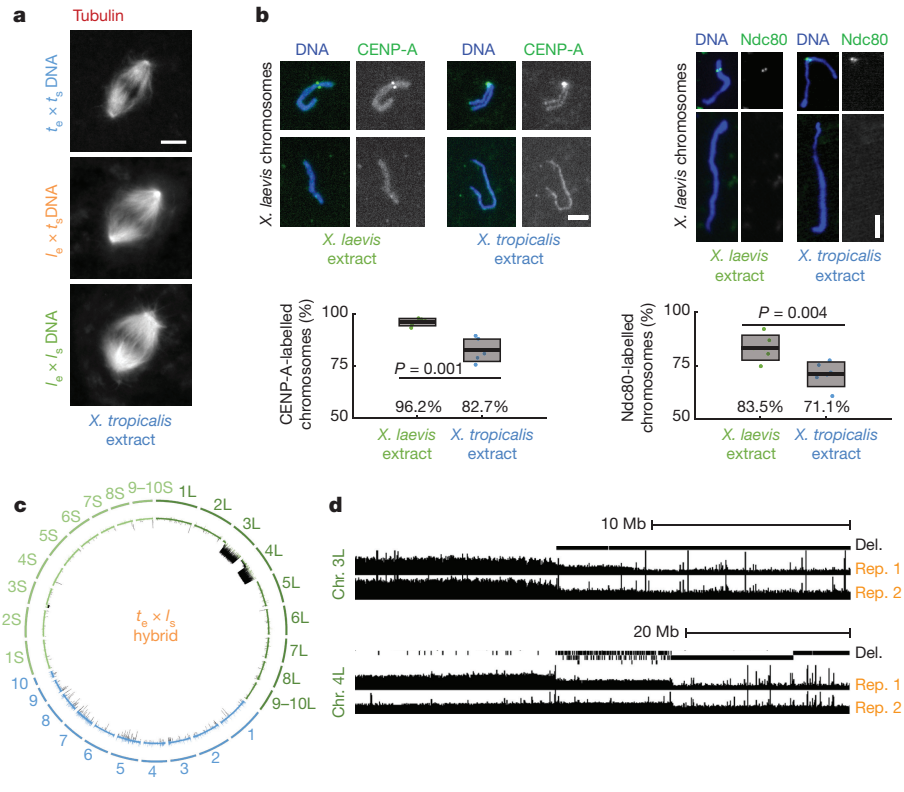

Figure 2 | Compatibility of *X. laevis* chromosomes with *X. tropicalis* cytoplasm. **a**, Fluorescence images of spindles formed around *X. tropicalis*, $l_e \times t_s$ hybrid, and *X. laevis* chromosomes in *X. tropicalis* egg extract. Scale bar, 10 μm. Quantification for $n = 147$, 103, and 156 spindles quantified for *X. tropicalis*, $l_e \times t_s$ hybrids, and *X. laevis* embryo nuclei, respectively, from three different egg extracts, is presented in Extended Data Fig. 1e. **b**, Fluorescence images of *X. laevis* chromosomes stained for CENP-A or Ndc80 following replication in *X. laevis* or *X. tropicalis* egg extract. CENP-A and Ndc80 labelling was quantified from six experiments (three biological replicates in two technical replicates), a total of $n = 1{,}792$ and $n = 1{,}959$ chromosomes, respectively, in *X. laevis* extract, and $n = 2{,}692$ and $n = 1{,}930$, respectively, in *X. tropicalis* extract. Scale bars, 5 μm. Box plots show the six experiment percentages as individual data points, their average as thick lines, and 1 s.d. as grey boxes. Ninety-five per cent confidence intervals are 96.2 ± 1.9% in *X. laevis* extract compared with 82.7 ± 5.7% in *X. tropicalis* extract for CENP-A, and 83.5 ± 6.1% compared with 71.1 ± 6.0% for Ndc80. *P* values were determined by two-tailed heteroscedastic *t*-test. **c**, Circle plot of whole-genome sequencing data for $t_e \times l_s$ hybrid embryos aligned and normalized to the genomes of *X. tropicalis* (blue) and *X. laevis* (green), with underrepresented genome regions in black. **d**, Expanded view of chromosome (Chr.) 3L and 4L breakpoints with deleted regions (Del.) indicated in two biological replicates (Rep.).

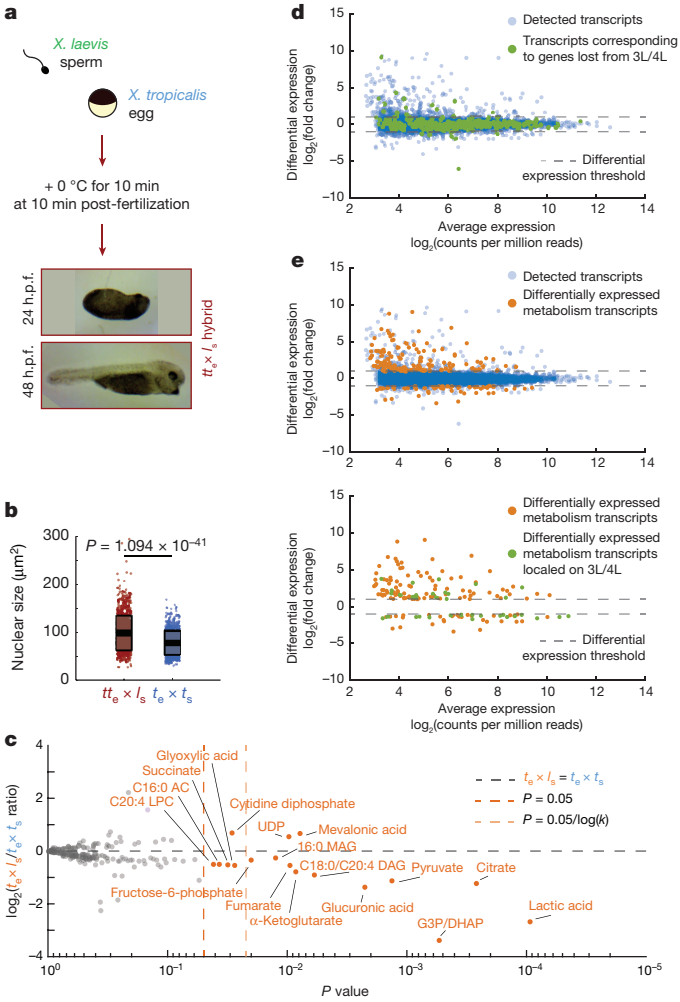

Figure 3 | Gene expression and metabolic changes preceding $t_e \times l_s$ hybrid embryo death. a, Schematic of polar body suppression experiment and images of $tt_e \times l_s$ rescued embryos 24 and 48 h.p.f. A total of nine $tt_e \times l_s$ embryos were obtained in four different experiments. **b**, Box plot of nuclear sizes ($n = 988$ nuclei from three $tt_e \times l_s$ embryos and $n = 777$ from three *X. tropicalis* embryos at stage 21) showing the average area as thick lines and 1 s.d. as grey boxes. Ninety-five per cent confidence intervals are $98.1 \pm 2.2\,\mu m^2$ for $tt_e \times l_s$ and $78.0 \pm 1.7\,\mu m^2$ for *X. tropicalis* embryos. *P* values were determined by two-tailed heteroscedastic *t*-test. **c**, Levels of 179 metabolites in *X. tropicalis* and $t_e \times l_s$ hybrid embryos 7 h.p.f. Levels were obtained from five samples from three independent fertilizations, each averaged and plotted as $\log_2$ of the ratio with the control (see Methods). *P* values were calculated using a two-tailed homoscedastic *t*-test. The average and 1 s.d. for the differentially represented metabolites are shown, and 95% confidence intervals given in Extended Data Fig. 3b. **d**, Differential gene expression between $t_e \times l_s$ and $t_e \times t_s$ (see Methods). All detected transcripts ($n = 8{,}379$) are plotted in blue. Transcripts corresponding to genes lost from chromosomes 3L and 4L ($n = 270$) are plotted in green. **e**, Differential expression of metabolism genes between $t_e \times l_s$ and $t_e \times t_s$ (see Methods). Differentially expressed metabolism transcripts ($n = 165$) are plotted in orange, all detected transcripts ($n = 8{,}379$) in blue (top), and differentially expressed metabolism transcripts located on chromosomes 3L and 4L ($n = 35$) in green (bottom).

(data not shown). Chromosome regions adjacent to breakpoints were heterogeneous in abundance (Fig. 2d), consistent with stochastic chromosome breakage and loss. Notably, major breakpoints localized to a gap in the genome assembly, indicating the presence of repetitive elements. Chromosome loss and partial deletion have been observed in non-viable hybrids in fish[13,14] and *Drosophila*[15], but the underlying mechanisms were unclear. Our results suggest that $t_e \times l_s$ hybrid incompatibility may be due to divergence of centromeric sequences, which are poorly characterized in *Xenopus* but known to evolve rapidly[16], or to other unidentified repetitive DNA elements that lead to chromosome instability and ultimately prevent kinetochore assembly on chromosomes 3L and 4L.

We next investigated the link between chromosome loss and $t_e \times l_s$ hybrid embryo death. Micronuclei in cancer cells accumulate DNA damage[17–19] and, in *Xenopus*, DNA damage was shown to trigger apoptosis at the onset of gastrulation[20]. As in cancer cells, micronuclei in $t_e \times l_s$ hybrid embryos often lost envelope integrity and contained damaged DNA (Extended Data Fig. 2a, b). However, $t_e \times l_s$ hybrid death did not resemble TdT-mediated dUTP nick end labelling (TUNEL)-positive apoptotic death induced by chemical inhibitors of DNA replication or protein synthesis in *X. tropicalis* embryos (Extended Data Fig. 2c, Extended Data Table 2 and Supplementary Videos 6 and 7). We hypothesized that chromosome loss could lead to cell death by affecting gene expression at zygotic genome activation. To assess the effects of blocking gene expression globally, we treated *X. tropicalis* embryos with the transcription initiation inhibitor triptolide and observed a phenotype reminiscent of the timing and manner of the catastrophic $t_e \times l_s$ hybrid embryo death, although lysis did not initiate from the vegetal side (Extended Data Table 2 and Supplementary Videos 8 and 9). To test whether altering gene dosage could rescue hybrid viability, we applied cold shock to the hybrid zygote to suppress polar body extrusion and introduce a second copy of the *X. tropicalis* genome. Although extremely inefficient, a total of nine triploid hybrid $tt_e \times l_s$ embryos were obtained in four separate experiments and survived to tailbud/tadpole stages (Fig. 3a). Rescued embryos possessed significantly higher DNA content than diploid *X. tropicalis* embryos at stage 21 (Fig. 3b), but whole-genome sequencing revealed that *X. laevis* DNA was eliminated by the tadpole stage (Extended Data Fig. 3a, Extended Data Table 3 and Supplementary Table 1). Our results link $t_e \times l_s$ hybrid inviability with altered gene expression that can be rescued with a second copy of the *X. tropicalis* genome, and indicate that $t_e \times l_s$ hybrid embryo inviability is caused by defects at the onset of zygotic genome activation, and not by DNA damage and apoptosis.

Because metabolite pools are known to become crucial before gastrulation[21], we subjected $t_e \times l_s$ hybrid embryos to metabolic profiling at 7 h post-fertilization (h.p.f.), just before the characteristic deformation preceding lysis. Levels of 17 out of 179 metabolites detected were significantly altered (Fig. 3c). Reduction in lactic acid, the final product of fermentation, and tricarboxylic acid cycle intermediates revealed that glycolytic metabolism was impaired in the cytoplasm of $t_e \times l_s$ hybrid embryos, which could in turn alter lipid metabolites including neutral lipids such as diacylglycerols and monoacylglycerols, as well as fatty-acid oxidation metabolites such as acyl carnitines (Extended Data Fig. 3b). While inhibition of mitochondrial ATP synthase led to cell cycle arrest at stage 9 (Supplementary Video 10), perturbing the early steps of glycolysis in $t_e \times t_s$ embryos induced cell death and lysis (Supplementary Video 11 and Extended Data Table 2). In particular, inhibition of glycogen phosphorylase to block the release of glucose from glycogen led to cell death at stage 9, initiating from the vegetal side of the embryo (Supplementary Video 12). These results are consistent with glycolytic defects as a primary cause of $t_e \times l_s$ hybrid embryo death. However, other defects that contribute to hybrid incompatibility could be masked by the abrupt cell lysis, such as conflicts between the paternal genome and maternal mitochondria[22,23].

To evaluate the link between the metabolic defects and specific chromosome loss, we used a statistical analysis[24] to classify the list of 1,803 genes mapped to the regions lost from chromosomes 3L and 4L in $t_e \times l_s$. We found that metabolic processes, particularly in glycolysis, were significantly over-represented (Extended Data Table 4). Transcriptome profiling of $t_e \times l_s$ hybrid embryos at 7 h.p.f. (Supplementary Table 2) revealed that although a large fraction of genes lost from chromosomes 3L and 4L were not differentially expressed compared with wild-type embryos (>92%; Fig. 3d), 27.1% of the differentially expressed genes related to metabolism (Fig. 3e, top), including

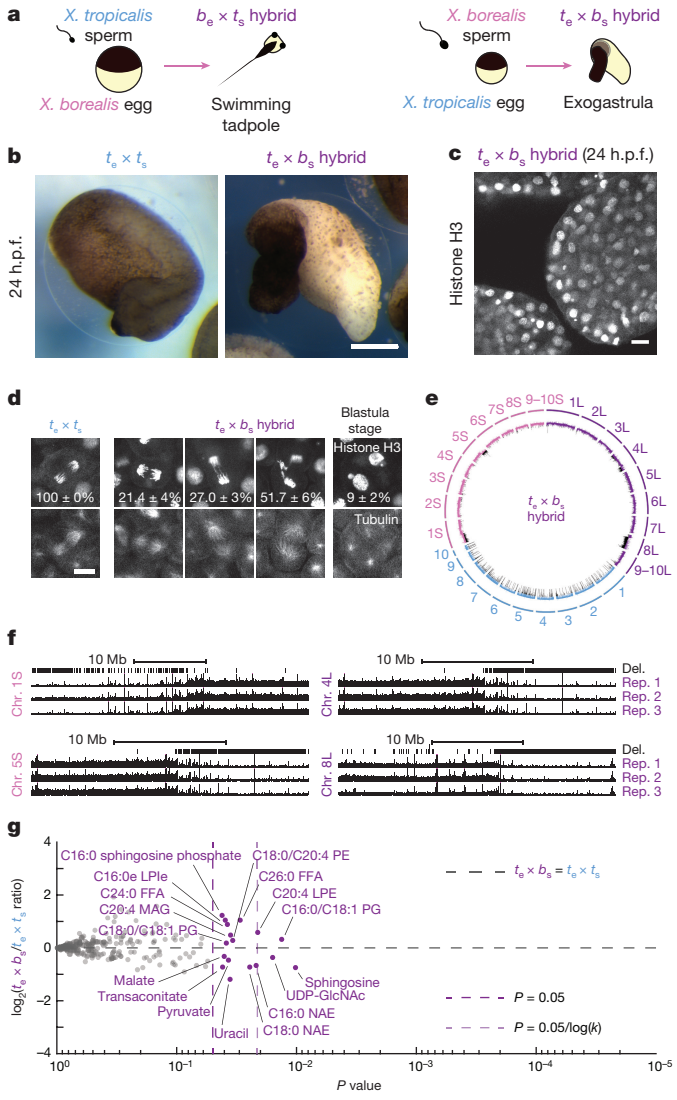

Figure 4 | Chromosomal loss in exogastrulating $t_e \times b_s$ hybrid embryos. a, Schematic of *X. borealis* and *X. tropicalis* cross-fertilization outcomes. **b**, Representative images of $t_e \times t_s$ compared with $t_e \times b_s$ embryos at 24 h.p.f. This result was reproduced in four separate experiments. Scale bar, 200 μm. **c**, Immunofluorescence image of $t_e \times b_s$ hybrid embryo at 24 h.p.f. showing nuclei and micronuclei. Similar defects at this stage were observed in six different embryos. **d**, Immunofluorescence images showing chromosome bridges, mis-segregating chromosomes, and micronuclei throughout $t_e \times l_s$ hybrid embryos. Scale bars, 20 μm. Quantification of $n = 33$ *X. tropicalis* and 63 $t_e \times b_s$ hybrid anaphases in $n = 6$ and 12 embryos, respectively, show a significant difference by Fisher's 2 × 3 contingency test ($P = 0$). Quantification of micronuclei in $t_e \times b_s$ hybrid embryos is detailed in Extended Data Fig. 4b. **e**, Circle plot of whole-genome sequencing data for $t_e \times b_s$ hybrid embryos aligned and normalized to the genomes of *X. tropicalis* (blue) and *X. borealis* (purple). Underrepresented genome regions (black) represent 9.674% of chromosome 4L, 74.66% of 8L, 4.71% of 1S, and 14.4% of 5S. **f**, Expanded view of chromosome 1S, 5L, 4L, and 8L breakpoints with deleted regions indicated in three biological replicates. **g**, Levels of 241 metabolites in *X. tropicalis* and $t_e \times b_s$ hybrid embryos 7 h.p.f. (see Methods). Levels were obtained from five samples from three independent fertilizations each, averaged and plotted as $\log_2$ of the ratio with the control (see Methods). *P* values were calculated using a two-tailed homoscedastic *t*-test. The average and 1 s.d. for the differentially represented metabolites are shown, and 95% confidence intervals given in Extended Data Fig. 3c. Note that few metabolites are altered significantly and are distinct from those altered in $t_e \times l_s$ hybrids (see Extended Data Fig. 3b, c).

PDK1 (pyruvate dehydrogenase kinase). Moreover, 36.7% of the significantly under-expressed metabolism genes are found on chromosomes 3L and 4L (Fig. 3e, bottom), including *GFPT1* (fructose-6-phosphate aminotransferase) and *HPDL* (4-hydroxyphenylpyruvate dioxygenase).

To further characterize the specificity and mechanism underlying $t_e \times l_s$ hybrid incompatibility, we compared the outcome of cross-fertilizations between *X. tropicalis* and another allotetraploid *Xenopus* species, *X. borealis*[25]. Analogous to hybridization between *X. laevis* and *X. tropicalis*, we observed that *X. borealis* eggs fertilized with *X. tropicalis* sperm ($b_e \times t_s$) were viable, whereas the reverse hybrid ($t_e \times b_s$) was not (Fig. 4a). However, the $t_e \times b_s$ embryos did not lyse, but exogastrulated and survived for hours with intact cells (Fig. 4b, c and Supplementary Video 13). Similar to $t_e \times l_s$, $t_e \times b_s$ embryos displayed chromosome loss through anaphase defects and formation of micronuclei (Fig. 4d and Extended Data Fig. 4a–c). Notably, whole $t_e \times b_s$ hybrid genome sequencing revealed that, although the loss was specific for the paternal genome as in the $t_e \times l_s$ hybrid, specific regions of four different *X. borealis* chromosomes were affected (Fig. 4e, f, Extended Data Table 3 and Supplementary Table 1). Furthermore, metabolomics of $t_e \times b_s$ embryos revealed a distinct profile with less severe alterations than observed for $t_e \times l_s$ (Fig. 4g).

Altogether, our results indicate that hybrid instability in *Xenopus* results primarily from post-zygotic conflicts between the maternal cytoplasm and the paternal genome that lead to loss of specific genomic regions and downstream gene dosage defects. These findings highlight the role of genome evolution and transmission in defining hybrid fates and speciation.

Online Content Methods, along with any additional Extended Data display items and Source Data, are available in the online version of the paper; references unique to these sections appear only in the online paper.

Received 1 November 2016; accepted 20 November 2017.
Published online 10 January 2018.

1. Seehausen, O. *et al.* Genomics and the origin of species. *Nat. Rev. Genet.* **15,** 176–192 (2014).
2. Presgraves, D. C. The molecular evolutionary basis of species formation. *Nat. Rev. Genet.* **11,** 175–180 (2010).
3. Session, A. M. *et al.* Genome evolution in the allotetraploid frog *Xenopus laevis*. *Nature* **538,** 336–343 (2016).
4. Brown, K. S. *et al. Xenopus tropicalis* egg extracts provide insight into scaling of the mitotic spindle. *J. Cell Biol.* **176,** 765–770 (2007).
5. Hirsch, N., Zimmerman, L. B. & Grainger, R. M. *Xenopus*, the next generation: *X. tropicalis* genetics and genomics. *Dev. Dyn.* **225,** 422–433 (2002).
6. Yanai, I., Peshkin, L., Jorgensen, P. & Kirschner, M. W. Mapping gene expression in two *Xenopus* species: evolutionary constraints and developmental flexibility. *Dev. Cell* **20,** 483–496 (2011).
7. Bürki, E. The expression of creatine kinase isozymes in *Xenopus tropicalis*, *Xenopus laevis laevis*, and their viable hybrid. *Biochem. Genet.* **23,** 73–88 (1985).
8. Narbonne, P., Simpson, D. E. & Gurdon, J. B. Deficient induction response in a *Xenopus* nucleocytoplasmic hybrid. *PLoS Biol.* **9,** e1001197 (2011).
9. Hamilton, L. Androgenic haploids of a toad, *Xenopus laevis*. *Nature* **179,** 159 (1957).
10. Goda, T. *et al.* Genetic screens for mutations affecting development of *Xenopus* tropicalis. *PLoS Genet.* **2,** e91 (2006).
11. Wühr, M. *et al.* Evidence for an upper limit to mitotic spindle length. *Curr. Biol.* **18,** 1256–1261 (2008).
12. Cheeseman, I. M. The kinetochore. *Cold Spring Harb. Perspect. Biol*. **6,** a015826 (2014).
13. Fujiwara, A., Abe, S., Yamaha, E., Yamazaki, F. & Yoshida, M. C. Uniparental chromosome elimination in the early embryogenesis of the inviable salmonid hybrids between masu salmon female and rainbow trout male. *Chromosoma* **106,** 44–52 (1997).
14. Sakai, C. *et al.* Chromosome elimination in the interspecific hybrid medaka between *Oryzias latipes* and *O. hubbsi*. *Chromosome Res.* **15,** 697–709 (2007).
15. Ferree, P. M. & Barbash, D. A. Species-specific heterochromatin prevents mitotic chromosome segregation to cause hybrid lethality in *Drosophila*. *PLoS Biol*. **7,** e1000234 (2009).
16. Kalitsis, P. & Choo, K. H. A. The evolutionary life cycle of the resilient centromere. *Chromosoma* **121,** 327–340 (2012).
17. Crasta, K. *et al.* DNA breaks and chromosome pulverization from errors in mitosis. *Nature* **482,** 53–58 (2012).
18. Hatch, E. M., Fischer, A. H., Deerinck, T. J. & Hetzer, M. W. Catastrophic nuclear envelope collapse in cancer cell micronuclei. *Cell* **154,** 47–60 (2013).

19. Terradas, M., Martín, M., Tusell, L. & Genescà, A. DNA lesions sequestered in micronuclei induce a local defective-damage response. *DNA Repair (Amst.)* **8,** 1225–1234 (2009).
20. Hensey, C. & Gautier, J. A developmental timer that regulates apoptosis at the onset of gastrulation. *Mech. Dev.* **69,** 183–195 (1997).
21. Vastag, L. *et al.* Remodeling of the metabolome during early frog development. *PLoS ONE* **6,** e16881 (2011).
22. Ma, H. *et al.* Incompatibility between nuclear and mitochondrial genomes contributes to an interspecies reproductive barrier. *Cell Metab.* **24,** 283–294 (2016).
23. Lee, H. Y. *et al.* Incompatibility of nuclear and mitochondrial genomes causes hybrid sterility between two yeast species. *Cell* **135,** 1065–1073 (2008).
24. Mi, H., Poudel, S., Muruganujan, A., Casagrande, J. T. & Thomas, P. D. PANTHER version 10: expanded protein families and functions, and analysis tools. *Nucleic Acids Res.* **44** (D1), D336–D342 (2016).
25. Schmid, M. & Steinlein, C. Chromosome banding in Amphibia. XXXII. The genus *Xenopus* (Anura, Pipidae). *Cytogenet. Genome Res.* **145,** 201–217 (2015).

Supplementary Information is available in the online version of the paper.

Acknowledgements We thank members of the Heald laboratory, present and past, for support and discussions. We thank the students who helped with some of the experiments: B. Castellano, J. Chen, S. Ramos, A. Sabillo, and K. Shih. We are also grateful to the Marine Biological Laboratory and the National *Xenopus* Resource for organizing the 2013 Advanced Imaging in *Xenopus* Workshop where several techniques used here were taught to R.G., and to J. Wallingford and A. Shindo for subsequent support. We thank the Welch, King, Harland, Rokhsar, Barton, and Fletcher laboratories at the University of California, Berkeley (UC Berkeley) for sharing reagents, materials, and expertise, as well as T. Stukenberg and A. Straight for providing us with the Ndc80 and CENP-A antibodies, respectively. We especially thank A. Mudd and D. Rokhsar for providing early access to the *X. borealis* genome assembly. This work used the Functional Genomics Laboratory, a QB3-Berkeley Core Research Facility at UC Berkeley as well as the Vincent J. Coates Genomics Sequencing Laboratory at UC Berkeley, supported by National Institutes of Health (NIH) S10 OD018174 Instrumentation Grant. The confocal microscopy performed in this work was done at the UC Berkeley CRL Molecular Imaging Center, supported by National Science Foundation DBI-1041078. R.G. was initially supported by EMBO long-term fellowship ALTF 836-2013 and for most of this project by Human Frontier Science Program long-term fellowship LT 0004252014-L. R.A. was supported in part by a National Science Foundation REU Summer Fellowship in 2014. R.H. was supported by NIH R35 GM118183 and the Flora Lamson Hewlett Chair. D.K.N. was supported by NIH R01 CA172667. M.K. was supported by UC Berkeley Department of Molecular and Cell Biology NIH training grant 4T32GM007232-40. T.K. was supported by Basic Science Research Program through the National Research Foundation of Korea funded by the Ministry of Science, ICT and Future Planning (NRF-2016R1C1B2009302), and the UNIST Research Fund (grant number 1.160060.01). G.J.C.V., I.V.K., and G.G. were supported by NIH R01 HD069344.

Author Contributions R.H. and R.G. designed the project. R.G. performed the molecular, cell, and developmental biology experiments, aided by R.A., and analysed the data. M.K., together with R.G., performed the experiments related to *X. borealis* and analysed the data. G.J.C.V., I.V.K., and G.G. prepared and analysed the hybrid genomes. B.M. and D.K.N. performed the metabolomic profiling of hybrids. T.K. and E.M.M. contributed to the transcriptome data analysis. R.G. prepared the figures and wrote the manuscript with R.H., incorporating feedback from all authors.

Author Information Reprints and permissions information is available at www.nature.com/reprints. The authors declare no competing financial interests. Readers are welcome to comment on the online version of the paper. Publisher's note: Springer Nature remains neutral with regard to jurisdictional claims in published maps and institutional affiliations. Correspondence and requests for materials should be addressed to R.H. (bheald@berkeley.edu).

Reviewer Information *Nature* thanks E. Amaya and the other anonymous reviewer(s) for their contribution to the peer review of this work.

METHODS

Chemicals. Unless otherwise stated, all chemicals were purchased from Sigma-Aldrich.

Frogs. All animal experimentation in this study was performed according to the Animal Use Protocol approved by the UC Berkeley Animal Care and Use Committee. Mature *X. laevis*, *X. tropicalis*, and *X. borealis* frogs were obtained from NASCO, or the National *Xenopus* Resource (Woods Hole). Female *X. laevis* (1–4 years old), *X. tropicalis* (6 months to 4 years old), and *X. borealis* (2–3 years old) frogs were ovulated with no harm to the animals with 6-, 3-, and 4-month rest intervals, respectively. To obtain testes, males (same age ranges) were euthanized by over-anaesthesia through immersion in double-distilled (dd)H_2O containing 0.15% MS222 (tricaine) neutralized with 5 mM sodium bicarbonate before dissection, and then frozen at −20 °C.

Experimental design. No statistical methods were used to pre-determine sample size sufficient to generate statistically significant differences. All attempts at replication were successful. All experiments were performed independently at least three times (biological replicates). *Xenopus* frogs were selected randomly from our colony for ovulation and fertilization experiments. The experiments were not randomized. The investigators were not blinded to allocation during experiments and outcome assessment.

***In vitro* fertilization and cross-fertilization.** *X. laevis* males were injected with 500 U of human chorionic gonadotropin hormone (hCG) 12–24 h before dissection and testes were stored at 4 °C in 1× MR (100 mM NaCl, 1.8 mM KCl, 2 mM $CaCl_2$, 1 mM $MgCl_2$, and 5 mM HEPES–NaOH pH 7.6) for 1–2 weeks. *X. tropicalis* and *X. borealis* males were injected with 250 U and 300 U, respectively, of hCG 12–24 h before dissection, and testes were collected in Leibovitz L-15 Medium (Gibco, Thermo Fisher Scientific) supplemented with 10% fetal bovine serum (FBS; Gibco) for immediate use.

For *X. tropicalis* egg-based embryos, *X. tropicalis* females were primed with 25 U of hCG 12–24 h before use and boosted with 250 U of hCG on the day of the experiment. As soon as the first eggs were laid (∼3 h after boosting), the *X. tropicalis* male was euthanized and dissected. Two *X. tropicalis* or *X. borealis* testes, or one-third of a *X. laevis* testis were each added to 1 ml of L-15 10% FBS. *X. tropicalis* females were squeezed gently to deposit eggs onto Petri dishes coated with 1.5% agarose in 1/10× MMR (1× MMR: 100 mM NaCl, 2 mM KCl, 2 mM $CaCl_2$, 1 mM $MgSO_4$, and 5 mM HEPES–NaOH pH 7.6, 0.1 mM EDTA). Testes were homogenized using scissors and a pestle in L-15 10% FBS. Any liquid in the Petri dishes was removed and the eggs were fertilized with 500 µl of sperm solution per dish. Eggs were swirled in the solution to separate them and incubated for 4 min with the dish slanted. Dishes were then flooded with ddH_2O, swirled, and incubated for 5–10 min. Buffer was exchanged for 1/10× MMR, the eggs incubated for 10 min, and jelly coats removed with a 3% cysteine solution (in ddH_2O–NaOH, pH 7.8). After extensive washing with 1/10× MMR (at least four times), embryos were incubated at 23 °C. At stage 2–3, fertilized embryos were sorted and placed in fresh 1/10× MMR within new Petri dishes coated with 1.5% agarose in 1/10× MMR.

For *X. laevis* egg-based embryos, *X. laevis* females were primed with 100 U of pregnant mare serum gonadotropin (PMSG, National Hormone and Peptide Program) at least 48 h before use and boosted with 500 U of hCG 14 h before the experiment. *X. laevis* females were squeezed gently to deposit eggs onto Petri dishes coated with 1.5% agarose in 1/10× MMR. Two *X. tropicalis* testes collected in L-15 10% FBS or one-third of a *X. laevis* testis were each added to 1 ml of ddH_2O and homogenized using scissors and a pestle. Any liquid in the Petri dishes was removed and the eggs were fertilized with 500 µl of sperm solution per dish. Eggs were swirled in the solution to individualize eggs as much as possible and incubated for 10 min. Dishes were flooded with 1/10× MMR, swirled, and incubated for 10–20 min. Jelly coats were removed with a 2% cysteine solution (in ddH_2O–NaOH, pH 7.8). After extensive washing (at least four times) with 1/10× MMR, embryos were incubated at 23 °C. At stage 2–3, fertilized embryos were sorted and placed in fresh 1/10× MMR in new Petri dishes coated with 1.5% agarose in 1/10× MMR.

For *X. borealis* egg-based embryos, *X. borealis* females were primed with 60 U of PMSG at least 48 h before use and boosted with 300 U of hCG 14 h before the experiment. Frogs were kept at 16 °C in 1/2× MMR. Eggs were picked from the tub and deposited onto Petri dishes coated with 1.5% agarose in 1/10× MMR. Two *X. tropicalis* or *X. borealis* testes were collected and homogenized using scissors and a pestle in L-15 10% FBS. Any liquid in the Petri dishes was removed and the eggs were fertilized with 500 µl of sperm solution per dish. Eggs were swirled in the solution to individualize eggs as much as possible and incubated for 10 min. Dishes were flooded with 1/10× MMR, swirled, and incubated for 10–20 min. Jelly coats were then removed with a 3% cysteine solution (in ddH_2O–NaOH, pH 7.8). After extensive washing (more than four times) with 1/10× MMR, embryos were incubated at 23 °C. At stage 2–3, fertilized embryos were sorted and placed in fresh 1/10× MMR in new Petri dishes coated with 1.5% agarose in 1/10× MMR.

All embryos were staged according to ref. 26.

Embryo chemical treatments and video imaging. Chemical treatments were performed in Petri dishes coated with exactly 5 ml of 1.5% agarose in 1/10× MMR covered with 10 ml 1/10× MMR for either regular incubations or video imaging for consistency. Concentrations were calculated relative to the covering volume of 1/10× MMR; no dilution within the volume in the agarose was assumed. Cycloheximide was added at a concentration of 0.1 mg ml^{-1} at stage 6.5 from 8 mg ml^{-1} stock in dimethylsulfoxide (DMSO). Hydroxyurea (Thermo Fisher Scientific) was added at a concentration of 30 mM at stage 3 from 600 mM stock in ddH_2O. Triptolide was added at a concentration of 25 µM at stage 2 from 25 mM stock in DMSO. Oligomycin was added at a concentration of 40 µM at stage 2 from 40 mM stock in DMSO. AP-III-a4 was added at a concentration of 30 µM at stage 2 from 1 mM stock in DMSO. Iodoacetic acid was added at a concentration of 50 mM at stage 2 from 1 M stock in ddH_2O. CP-91,149 was added at a concentration of 270 µM at stage 2 from 30 mM stock in DMSO. Corresponding volumes of DMSO or ddH_2O were added to controls.

Imaging dishes were prepared using an in-house PDMS mould designed to print a pattern of 0.9 mm large wells in agarose that allowed us to image six *X. tropicalis* embryos simultaneously within the 3 mm × 4 mm camera field of view for each condition. Embryos were imaged from stage 2–3. Treatment and control videos were taken simultaneously using two AmScope MD200 USB cameras (AmScope), each mounted on an AmScope SE305R stereoscope. Time-lapse movies were acquired at a frequency of one frame every 10 s for 20 h and saved as Motion JPEG using a MATLAB (The MathWorks) script. Movie post-processing (cropping, concatenation, resizing, and addition of scale bar) was done using MATLAB and Fiji[27]. All MATLAB scripts written for this study are available upon request. Two of the scripts used here were obtained through the MATLAB Central File Exchange: 'videoMultiCrop' and 'concatVideo2D' by 'Nikolay S'.

Embryo ploidy manipulations. To generate *X. tropicalis* haploid embryos ($t_e \times [t_s]$ and $t_e \times [l_s]$), fertilizations were conducted as detailed above with slight modifications to accommodate sperm ultraviolet-irradiation. Two *X. tropicalis* testes or one-third of a *X. laevis* testis were each added to 1.1 ml of L-15 10% FBS. Testes were homogenized using scissors and a pestle, and the solutions spun briefly using a benchtop centrifuge to pellet the tissue. One millilitre of supernatant was transferred into a glass Petri dish and irradiated within a Stratalinker UV-Crosslinker (Stratagene) with 50,000 µJ for *X. tropicalis* sperm or 2× 30,000 µJ for *X. laevis* sperm, swirling the solution in between the two irradiations. *X. tropicalis* eggs freshly squeezed onto Petri dishes coated with 1.5% agarose in 1/10× MMR were then fertilized with 500 µl of irradiated sperm solution per dish and processed as described above.

To generate $[t_e] \times l_s$ cybrid embryos and the haploid $[t_e] \times t_s$ controls, fertilizations were conducted as detailed above with slight modifications to accommodate for the ultraviolet-irradiation of the eggs. Two *X. tropicalis* testes or two-thirds of a *X. laevis* testis were each added to 1.1 ml of L-15 10% FBS. *X. tropicalis* females were squeezed gently to deposit eggs onto Petri dishes coated with 1.5% agarose in 1/10× MMR. Excess liquid was removed, eggs were swirled with a pestle to form a monolayer of properly oriented eggs, and immediately irradiated in a Stratalinker UV-Crosslinker (Stratagene) 2× with 40,000 µJ. Testes were homogenized using scissors and a pestle during the irradiation of the eggs. As soon as they were irradiated, the eggs were fertilized with 500 µl of sperm solution per dish and processed as described above.

To prevent polar body formation in either $tt_e \times t_s$ or $tt_e \times l_s$ experiments, fertilizations were conducted as detailed above with slight modifications to accommodate cold treatment. Fertilizations were performed within dishes coated with only 1–1.5 ml, instead of 5 ml, of 1.5% agarose in 1/10× MMR to accelerate cooling. Following the 4-min incubation with sperm, dishes were flooded with ddH_2O, swirled, and incubated for exactly 5 min. Buffer was then exchanged for ice-cold 1/10× MMR, the dishes transferred into a pipette tip box lid placed in a slushy ice bucket, and the eggs incubated for 10 min. The dishes were then removed from the bucket and the cold buffer was exchanged for RT 1/10× MMR. After 20 min, the jelly coat was removed with a 3% cysteine solution (in ddH_2O–NaOH, pH 7.8) and the embryos processed as described above.

Animal cap assay. At stage 8, embryos were placed in Danilchik's for Amy Medium (DFA medium; 53 mM NaCl, 5 mM Na_2CO_3, 4.5 mM potassium gluconate, 32 mM sodium gluconate, 1 mM $CaCl_2$, 1 mM $MgSO_4$, pH 8.3, 1 g l^{-1} bovine serum albumin and 0.8% Antibiotic Antimycotic Solution) for surgery. Using Dumostar-Biology 55 forceps (Dumont), the vitelline membrane was removed and the animal cap was isolated from the embryo. The caps were finally transferred to a new dish or a chamber containing fresh DFA medium for imaging.

mRNA, embryo microinjection, and animal cap confocal microscopy. Plasmids for expression of EB3–GFP and histone H2B–RFP mRNAs were obtained at the

2013 Advanced Imaging in *Xenopus* Workshop from the Wallingford laboratory. The mRNAs were synthetized using an mMessage mMachine SP6 Transcription Kit (Ambion, Thermo Fisher Scientific) following the supplier's protocol. The mRNAs were purified using phenol–chloroform extraction, resuspended in ddH_2O, aliquoted, and stored at −80 °C.

At stage 2, $t_e \times l_s$ hybrid embryos were transferred to 1/9× MMR 3% Ficoll. A solution containing 50 pg nl^{-1} of H2B–RFP mRNA and 100 pg nl^{-1} of EB3–GFP mRNA, concentrations that allowed us to image fluorescent signal as early as stage 9, was loaded into a needle pulled from a 1-mm glass capillary tube (TW100F-4, World Precision Instruments) using a P-87 Micropipette Puller (Sutter Instrument). Embryos were placed in a mesh-bottomed dish and microinjected in both blastomeres with 1 nl of the mRNA solution using a Picospritzer III microinjection system (Parker) equipped with a MM-3 micromanipulator (Narishige). Injected embryos were transferred to a new dish and incubated at 23 °C in 1/9× MMR 3% Ficoll until stage 8, when they were processed for animal cap isolation as described above. Caps were placed in a chamber filled with DFA medium made using 1 cm × 1 cm Gene Frames (Thermo Fisher Scientific) between a slide and a coverslip (Thermo Fisher Scientific) for confocal microscopy.

Embryo whole-mount immunofluorescence. At desired stages, embryos were fixed for 1–3 h using either MAD fixative (two parts of methanol (Thermo Fisher Scientific), two parts of acetone (Thermo Fisher Scientific), one part of DMSO) for most antibodies or MEMFA fixative (0.1 M MOPS pH 7.4, 2 mM EGTA, 1 mM $MgSO_4$, 3.7% formaldehyde) for the γH2A.X antibody. After fixation, embryos were dehydrated in methanol and stored at −20 °C. Embryos were then processed as previously described[28] with some modifications. Following gradual rehydration in 0.5× SSC (1× SSC: 150 mM NaCl, 15 mM Na citrate, pH 7.0), embryos were bleached with 1–2% H_2O_2 (Thermo Fisher Scientific) in 0.5× SSC containing 5% formamide for 2–3 h under light, then washed in PBT, a PBS solution containing 0.1% Triton X-100 (Thermo Fisher Scientific), and 2 mg ml^{-1} bovine serum albumin. Embryos were blocked in PBT supplemented with 10% goat serum (Gibco, Thermo Fisher Scientific) and 5% DMSO for 1–3 h and incubated overnight at 4 °C in PBT supplemented with 10% goat serum and the primary antibodies. We used different combinations of the following antibodies: 1:500 mouse anti-β-tubulin (E7; Developmental Studies Hybridoma Bank), 1:500 rabbit anti-histone H3 (ab1791; Abcam), 1:500 rabbit anti-lamin B1 (ab16048; Abcam), and 1:500 mouse anti-phospho-histone H2A.X (05-636; EMD Millipore, Merck KGaA). Embryos were then washed 4 × 2 h in PBT and incubated overnight in PBT supplemented with 1:500 goat anti-mouse or goat anti-rabbit secondary antibodies coupled either to Alexa Fluor 488 or 568 (Invitrogen, Thermo Fisher Scientific) and with 1:200 YO-PRO iodide (Thermo Fisher Scientific) if the use of anti-histone H3 antibody as primary was not possible. Embryos were then washed 4 × 2 h in PBT and gradually dehydrated in methanol. Embryos were finally cleared in Murray's clearing medium (two parts of benzyl benzoate, one part of benzyl alcohol). Embryos were placed either in a chamber made using a flat nylon washer (Grainger) attached with nail polish (Sally Hansen) to a slide and covered by a coverslip or a chamber made of silicon grease (Beckman coulter) between slide and coverslip, and filled with Murray's clearing medium for confocal microscopy.

Confocal microscopy, micronuclei, and nuclear size quantification. Confocal microscopy was performed on a Zeiss LSM 780 NLO AxioExaminer using the Zeiss Zen software. For animal cap live imaging, histone H2B–RFP and EB3–GFP signals were imaged on a single plane with a frame size of 1,024 pixels × 1,024 pixels every 5 s using a Plan-Apochromat 40×/1.4 oil objective and laser power of 22%. For imaging of histone H3, embryos were imaged using a Plan-Apochromat 20×/1.0 water objective and laser power of 12%, on multiple 1,024 × 1,024 pixel plans spaced of 0.68 μm in Z. For characterization of the micronuclei (lamin B1 and γH2A-X), embryos were imaged using a Plan-Apochromat 63×/1.40 oil objective and laser power of 12%, on multiple plans spaced 0.38 μm in Z. Images are mean averages of two scans with a depth of 16 bits. Pinhole size was always chosen to correspond to 1 Airy unit.

Micronuclei were quantified at stages 4, 6, 7, 8, and 9 as the number of observed micronuclei in the dataset divided by the number of nuclei in the dataset. The number of micronuclei at all stages and of nuclei at stages 4 and 6 were counted manually in Fiji. The number of nuclei at stages 7, 8, and 9 was determined automatically through histone H3 fluorescence signal segmentation using Imaris (Bitplane). Nuclear area in $tt_e \times t_s$, *X. tropicalis* and $t_e \times [t_s]$ was measured in Fiji using the ellipse tool. From this, we calculated the diameter of a circle of the same area, a value that we could directly compare to the cell size determined through the measurement of the cell diameter at the nucleus central plan.

Embryo nuclei purification. Embryo nuclei were prepared as previously described[29] from *X. tropicalis*, $l_e \times t_s$ hybrid, and *X. laevis* embryos. In brief, embryos were arrested at stage 8 in late interphase using 150 μg ml^{-1} cycloheximide in 1/10× MMR for 60 min. Then they were washed several times in ELB (250 mM sucrose, 50 mM KCl, 2.5 mM $MgCl_2$, and 10 mM HEPES pH 7.8) supplemented with LPC (10 μg ml^{-1} each leupeptin, pepstatin, chymostatin), cytochalasin D (100 μg ml^{-1}), and cycloheximide (100 μg ml^{-1}), packed in a tabletop centrifuge at 200*g* for 1 min, crushed with a pestle, and centrifuged at 10,000*g* for 10 min at 16 °C. The cytoplasmic extract containing endogenous embryonic nuclei was collected, supplemented with 8% glycerol, aliquoted, frozen in liquid nitrogen, and stored at −80 °C.

***Xenopus* egg extracts and related methods.** *X. laevis*[30] and *X. tropicalis*[4] metaphase-arrested egg extracts were prepared and spindle reactions conducted as previously described.

To reconstitute spindle assembly, stage 8 embryo nuclei were used as a source of DNA. Aliquots were thawed, resuspended in 1 ml of ELB, and spun at 1,600*g* for 5 min at room temperature. Pelleted nuclei were resuspended in 25 μl of fresh *X. tropicalis* extract and incubated at room temperature.

To examine kinetochore assembly, *X. laevis* sperm nuclei, prepared as previously described[31], were used as a source of DNA in both *X. laevis* and *X. tropicalis* egg extracts. Cycled chromosomes were prepared and spun-down[30], then processed for immunofluorescence as previously described[32]. In brief, the coverslips were incubated for 1 min in cold methanol, washed with PBS+NP40, and blocked overnight in PBS + 5% bovine serum albumin at 4 °C. The anti-Ndc80 (1:300 dilution, Stukenberg laboratory) or the anti-CENP-A (1:500 dilution, Straight laboratory) rabbit antibodies were added for 1 h. After washing with PBS+NP40, the coverslips were incubated with 1:1,000 anti-rabbit antibody coupled to Alexa Fluor 488 (Invitrogen, Thermo Fisher Scientific) for 30 min and then with 1:1,000 Hoechst for 5 min. The coverslips were finally washed and mounted for imaging. Each presented dataset was obtained from three different egg extracts with technical duplicates for each.

Spindles and chromosomes were imaged using micromanager software[33] with an Olympus BX51 microscope equipped with an ORCA-ER or an ORCA-II camera (Hamamatsu Photonics), and with an Olympus UPlan FL 40× air objective. Spindle measurements were made using Fiji and the spindle tubulin intensity line scan using an automated Java ImageJ plugin developed by X. Zhou (https://github.com/XiaoMutt/AiSpindle).

TUNEL assay. Embryos were fixed in MEMFA as described for embryo whole-mount immunofluorescence and processed as previously described[20] with minor modifications. In brief, after gradual rehydration, embryos were bleached with 1–2% H_2O_2 in 0.5× SSC containing 5% formamide for 1–2 h under light. After washes in PBS, embryos were incubated in 1× terminal deoxynucleotidyl transferase (TdT) buffer for 1 h and then overnight in TdT Buffer supplemented with 150 U ml^{-1} of TdT enzyme (Invitrogen, Thermo Fisher Scientific) and 1 pmol μl^{-1} Digoxigenin-11-dUTP (Roche). After washes in 1 mM EDTA/PBS at 65 °C, in PBS, and then in MAB (100 mM maleic acid, 150 mM NaCl, pH 7.5), embryos were blocked for 1 h in 2% Blocking Reagent (Roche) in MAB and then incubated overnight at 4 °C in 2% Blocking Reagent in MAB supplemented with 1:3,000 anti-Digoxigenin AP antibody (Roche). After washes in MAB and in AP Buffer (100 mM Tris, pH 9.5, 50 mM $MgCl_2$, 100 mM NaCl, 0.1% Tween 20, 2 mM levamisol), embryos were stained with NBT/BCIP (nitro-blue tetrazolium/5-bromo-4-chloro-3-indolyl phosphate; Promega) diluted in AP buffer. Reactions were stopped in MAB and embryos fixed overnight in Bouin's solution. After washes in 70% buffered ethanol and in methanol, embryos were imaged in methanol with the ToupView software (ToupTek) using an AmScope MD200 USB camera mounted on M5 stereoscope (Wild Heerbrugg).

Nucleic acid isolation, library construction, and sequencing. For genomic DNA, embryos at desired stages were incubated overnight in lysis buffer (50 mM Tris-HCl, 5 mM EDTA, 100 mM NaCl, 0.5% SDS) containing 250 μg ml^{-1} Proteinase K (Roche). DNA was isolated using phenol–chloroform extraction and ethanol precipitation. To isolate RNAs, embryos at desired stages were homogenize mechanically in TRIzol (Thermo Fisher Scientific) using up to a 30-gauge needle and processed according to the supplier's instructions. After resuspension in nuclease-free H_2O, RNAs were cleaned up using RNeasy kit (Qiagen) with on-column DNA digestion, following the supplier's protocol.

Libraries were constructed at the Functional Genomics Laboratory (FGL), a QB3-Berkeley Core Research Facility at UC Berkeley. For genomic DNA, an S220 Focused-Ultrasonicator (Covaris) was used to fragment DNA. The fragmented DNA was cleaned and concentrated with an MinElute PCR Purification kit (Qiagen). The library preparation was done on an Apollo 324 with PrepX ILM 32i DNA Library Kits (WaferGen Biosystems), and seven cycles of PCR amplification were used for library fragment enrichment. For RNAs, mRNA enrichment was performed on total RNA using polyA selection with an Invitrogen Dynabeads mRNA Direct kit. The library preparation was done on an Apollo324 with PrepX RNA-seq Library Prep Kits (WaferGen Biosystems), and 13 cycles of PCR amplification were used for index addition and library fragment enrichment.

Sequencing was performed by the Vincent J. Coates Genomics Sequencing Laboratory at UC Berkeley. All samples were run as 100 paired-end HiSeq4000

lanes, pooled equimolar after quantification using KAPA Illumina Library quantification qPCR reagents on the BioRad CFX connect. Demultiplexing was performed to allow a single mismatch with Illumina's bcl2fastq version 2.17 software.

Genomic DNA sequencing analysis and deletion detection in hybrids. DNA sequencing reads were mapped to a *X. laevis*–*X. tropicalis* hybrid genome (Xenla9.1 and Xentro9.0) or a *X. borealis*–*X. tropicalis* hybrid genome (Xbo_04Apr2017 (A. Mudd and D. Rokhsar, unpublished observations) and Xentro9.0) using bwa mem (version 0.7.10-r789) with default settings. Duplicate reads were marked using bamUtil version 1.0.2.

Deletions in $t_e \times l_s$ and $l_e \times t_s$ hybrids were called by comparing local DNA sequencing read coverage between hybrid ($t_e \times l_s$ or $l_e \times t_s$) and parental ($t_e \times t_s$ or $l_e \times l_s$) genomes. The read coverage was determined in 10-kb regions, with a 2-kb sliding window across the genome. For each 10-kb region, we calculated the reads per kilobase per million reads (RPKM) in $t_e \times l_s$, $l_e \times t_s$, $t_e \times t_s$, and $l_e \times l_s$ sequencing tracks. The ratio of median RPKM values in retained regions had a non-zero baseline as expected because of a different size of hybrid and parental genomes. The ratio cut-off for deleted regions was set accordingly at fourfold and sixfold for *X. laevis* and *X. tropicalis* sequences, respectively. Lost regions overlapping for more than 30% of their length with gaps were removed and regions within 10 kb of each other were merged. Lost genes were analysed using the PANTHER database[24]. Because PANTHER only provided adjusted *P* values for fold enrichment based on binomial tests, we additionally estimated the 95% confidence interval for each enriched pathway using binom.test() function in R (version 3.2.2).

Deletions in $t_e \times b_s$ hybrids were called by identifying reduced genomic DNA signal in $t_e \times b_s$. The RPKM read coverage was determined in 10-kb regions, with a 2-kb sliding window across the genome. Regions with median $\log_{10}$ RPKM less than −1.25 in the *X. tropicalis* genome and −1.15 in the *X. borealis* genome were marked as deleted. Lost regions overlapping for more than 30% of their length with gaps were removed and regions within 10 kb of each other were merged.

RNA sequencing analysis. We mapped RNA sequencing reads to the combined primary transcripts of *X. laevis* (JGIv18pV4) and *X. tropicalis* (JGIv91) using bwa mem (version 0.7.10), and discarded all reads mapped in multiple targets for further analysis. To use human gene annotation, which is more comprehensive than *Xenopus*, we transferred the expression level of these species to human orthologues. On the basis of the best BLASTP hit to human longest protein sequences (from EnsEMBL version 80), we merged the read counts of *X. laevis* and *X. tropicalis* genes to corresponding human genes, then performed differential expression analysis with EdgeR[34]. An adjusted *P* value criterion of less than 0.05 was applied to determine the significance of differential expression. To estimate the 95% confidence interval of log-scale fold change, we used limma[35] (version 3.28.10). Results of both EdgeR and Limma analyses are presented in Supplementary Table 2. For metabolic gene analysis, we used the list of metabolic genes obtained from the PANTHER database[24].

Metabolomic profiling. Seven hours post-fertilization, $t_e \times l_s$ hybrid, $t_e \times b_s$ hybrid, and respective *X. tropicalis* control embryos were collected from three independent fertilizations, always using eggs from the same female between the $t_e \times l_s$ hybrid or the $t_e \times b_s$ hybrid, and its *X. tropicalis* control. Five samples of 8 embryos each for non-polar lipid metabolites and 12 embryos each for polar metabolites were rinsed twice in filtered PBS and frozen in liquid nitrogen. Non-polar lipid metabolites from the eight embryos were extracted in 3 ml of 2:1 chloroform:methanol and 1 ml of PBS with inclusion of internal standards C12 monoalkylglycerol ether (10 nmol, Santa Cruz Biotechnology) and pentadecanoic acid (10 nmol). Organic and aqueous layers were separated by centrifugation at 1,000*g* for 5 min and the organic layer was collected, dried under a stream of nitrogen, and dissolved in 120 µl chloroform. Polar metabolites were extracted from the 12 embryos in 180 µl of 40:40:20 (acetonitrile:MeOH:H_2O) with inclusion of internal standard D3N15 serine (50 nM, Cambridge Isotope Laboratories, DNLM-6863). Samples were disrupted by sonication then centrifuged at 21,000*g* for 10 min and the supernatant was collected for analysis. Metabolites were separated by liquid chromatography, and MS analysis was performed with an electrospray ionization source on an Agilent 6430 QQQ LC-MS/MS (Agilent Technologies). The capillary voltage was set to 3.0 kV, and the fragmentor voltage was set to 100 V. The drying gas temperature was 350 °C, the drying gas flow rate was 10 l min^{-1}, and the nebulizer pressure was 35 p.s.i. Metabolites were identified by single-reaction monitoring of the transition from precursor to product ions at associated optimized collision energies and retention times as previously described[36]. Metabolites were quantified by integrating the area under the curve, then normalized to internal standard values and tissue weight. Metabolite levels are expressed as relative abundances compared with controls. *P* values were calculated using a two-tailed homoscedastic *t*-test. Significance was analysed for an $\alpha = 0.05$ threshold as well as that with a Bonferroni-like correction to account for multiple hypothesis comparison. Strict Bonferroni correction is highly conservative and often results in increased type II errors (failing to acknowledge a real effect) and several alternatives exist. Because we compared around 200 compounds between two types of embryo, each with five replicates, we used a penalized Bonferroni correction, and divided the α threshold value by the logarithm of the number of tests ($\alpha/\log(k)$) to decrease the risk of a type II error.

Data availability. All genomic and transcriptomic data generated for this study are available from public databases: stage 9 $t_e \times l_s$ hybrid whole-genome sequencing data (NCBI Sequence Read Archive SRP124316) and corresponding stage 9 *X. laevis*, *X. tropicalis*, and $l_e \times t_s$ hybrid controls (NCBI Gene Expression Omnibus GSE92382), tailbud and tadpole stage $tt_e \times l_s$ hybrid whole-genome sequencing data (NCBI Sequence Read Archive SRP124316), stage 9 $t_e \times b_s$ hybrid whole-genome sequencing data (NCBI Sequence Read Archive SRP124316), and 7 h.p.f. *X. tropicalis* and $t_e \times l_s$ hybrid transcriptome RNA sequencing data (NCBI Gene Expression Omnibus GSE106157).

Code availability. MATLAB scripts were written to acquire and process embryo live-imaging movies. All these scripts are available from the corresponding author upon request. Two MATLAB scripts used here for movie cropping and concatenation were obtained through the MATLAB Central File Exchange: 'videoMultiCrop' and 'concatVideo2D' by 'Nikolay S'. The automated spindle tubulin intensity line scan Java ImageJ plugin developed by X. Zhou is available on GitHub (https://github.com/XiaoMutt/AiSpindle).

26. Nieuwkoop, P. D & Faber, J. *Normal Table of Xenopus laevis (Daudin)* (Garland, 1994).
27. Schindelin, J. *et al.* Fiji: an open-source platform for biological-image analysis. *Nat. Methods* **9,** 676–682 (2012).
28. Lee, C., Kieserman, E., Gray, R. S., Park, T. J. & Wallingford, J. Whole-mount fluorescence immunocytochemistry on *Xenopus* embryos. *CSH Protoc.* **2008,** pdb.prot4957 (2008).
29. Levy, D. L. & Heald, R. Nuclear size is regulated by importin α and Ntf2 in *Xenopus*. *Cell* **143,** 288–298 (2010).
30. Maresca, T. J. & Heald, R. Methods for studying spindle assembly and chromosome condensation in *Xenopus* egg extracts. *Methods Mol. Biol.* **322,** 459–474 (2006).
31. Murray, A. W. Cell cycle extracts. *Methods Cell Biol.* **36,** 581–605 (1991).
32. Hannak, E. & Heald, R. Investigating mitotic spindle assembly and function *in vitro* using *Xenopus* laevis egg extracts. *Nat. Protocols* **1,** 2305–2314 (2006).
33. Edelstein, A. D. *et al.* Advanced methods of microscope control using μManager software. *J. Biol. Methods* **1,** 10 (2014).
34. Robinson, M. D., McCarthy, D. J. & Smyth, G. K. edgeR: a Bioconductor package for differential expression analysis of digital gene expression data. *Bioinformatics* **26,** 139–140 (2010).
35. Ritchie, M. E. *et al.* limma powers differential expression analyses for RNA-sequencing and microarray studies. *Nucleic Acids Res.* **43,** e47 (2015).
36. Louie, S. M. *et al.* GSTP1 is a driver of triple-negative breast cancer cell metabolism and pathogenicity. *Cell Chem. Biol.* **23,** 567–578 (2016).

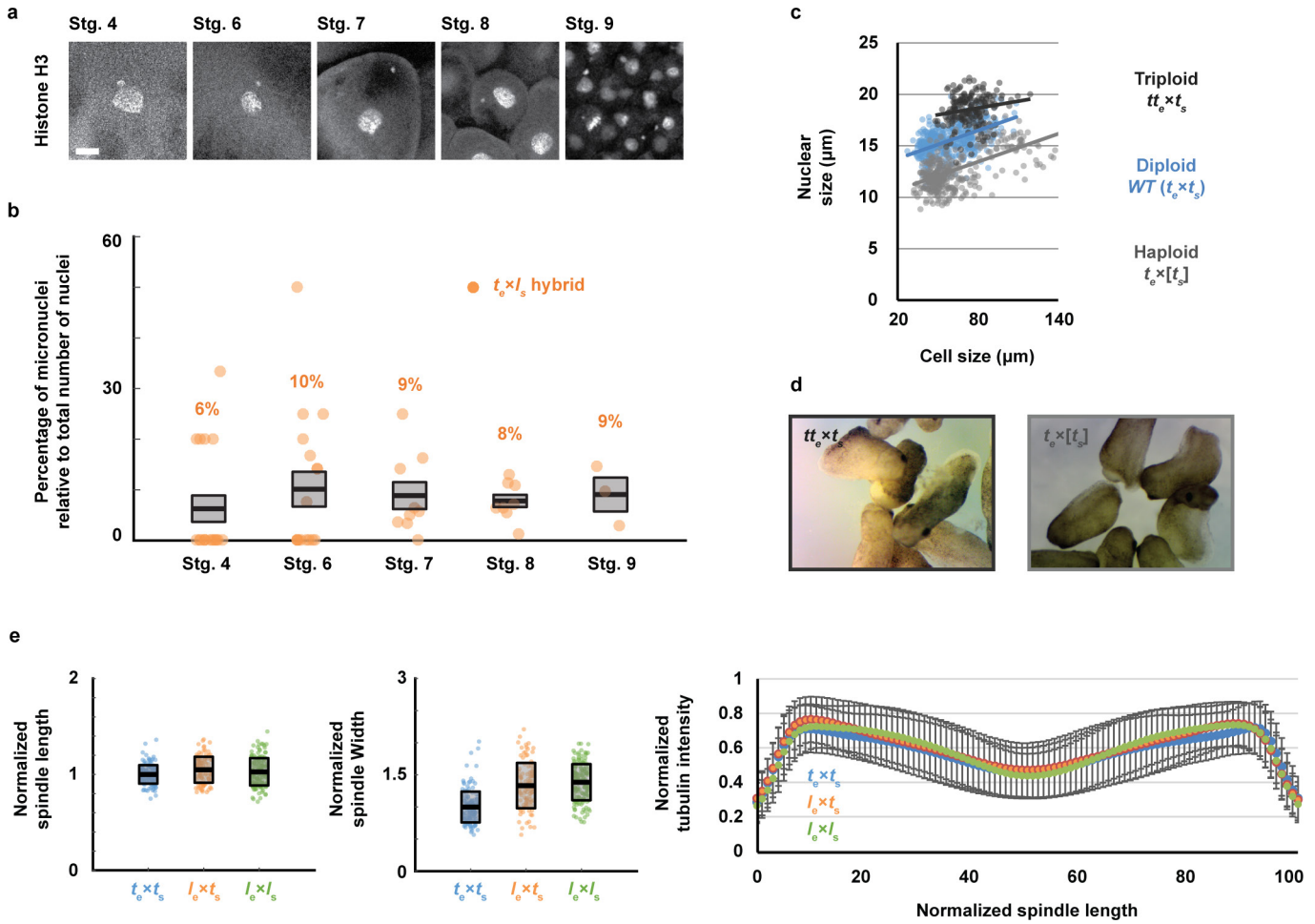

Extended Data Figure 1 | Occurrence of micronuclei, role of ploidy and spindle architecture. a, Micronuclei in $t_e \times l_s$ hybrid embryos at various developmental stages. Whole-mount embryo immunofluorescence was performed in $t_e \times l_s$ hybrid embryos using anti-histone H3 antibody at stages 4, 6, 7, 8, and 9 and quantified in **b**. Scale bar, 10 μm. **b**, Quantification of micronuclei in $t_e \times l_s$ hybrid embryos. The percentage of micronuclei was calculated as the number of micronuclei in the imaged portion of the embryo divided by the total number of nuclei in the same imaged portion. The average percentage for multiple embryos at stage 4 ($n = 18$ $t_e \times l_s$ hybrid embryos (individual dots) with a total of 63 nuclei), stage 6 ($n = 17/115$), stage 7 ($n = 9/322$), stage 8 ($n = 8/1119$), and stage 9 ($n = 3/2004$) from three independent experiments is shown as thick line. Grey boxes indicate 1 s.e.m. Control *X. tropicalis* embryos from the same mothers were analysed but no micronuclei were observed at any stages. **c**, Nuclear size in *X. tropicalis* embryos with varying ploidy. Nuclear size relative to cell size (diameters in micrometres) is plotted for triploid ($tt_e \times t_s$; dark grey, $n = 175$ nuclei from six embryos), diploid (*X. tropicalis*, $t_e \times t_s$; blue, $n = 453/9$), and haploid ($t_e \times [t_s]$; light grey, $n = 346/16$) embryos. Each dot indicates an individual data point and the solid lines indicate a linear fit. **d**, *X. tropicalis* embryos with varying ploidy at tailbud stage. Images of triploid ($tt_e \times t_s$; left) and haploid ($t_e \times [t_s]$; right) tailbuds were taken under identical conditions. Similar observations were over three independent experiments. **e**, Size and microtubule distribution in *X. tropicalis* spindles assembled from different embryo nuclei DNA ($n = 147$, 103, and 156 spindles quantified for *X. tropicalis*, $l_e \times t_s$ hybrids, and *X. laevis* embryo nuclei, respectively, from three different egg extracts). Spindle length (left) and width (middle) were normalized to the *X. tropicalis* control, averages are shown as thick black lines, and the grey boxes indicate 1 s.d. Ninety-five per cent confidence intervals for lengths are 1 ± 0.02 for $t_e \times t_s$, 1.05 ± 0.03 for $l_e \times t_s$, and 1.03 ± 0.02 for $l_e \times l_s$, and for widths are 1 ± 0.04, 1.3 ± 0.07, and 1.4 ± 0.04. Line scans of rhodamine-tubulin signal along spindle length were taken (right). Spindle lengths were normalized to 100% and tubulin intensities were normalized within datasets. The average intensities are plotted for the three spindle types, error bars indicate s.d., and colours are as in Fig. 2a.

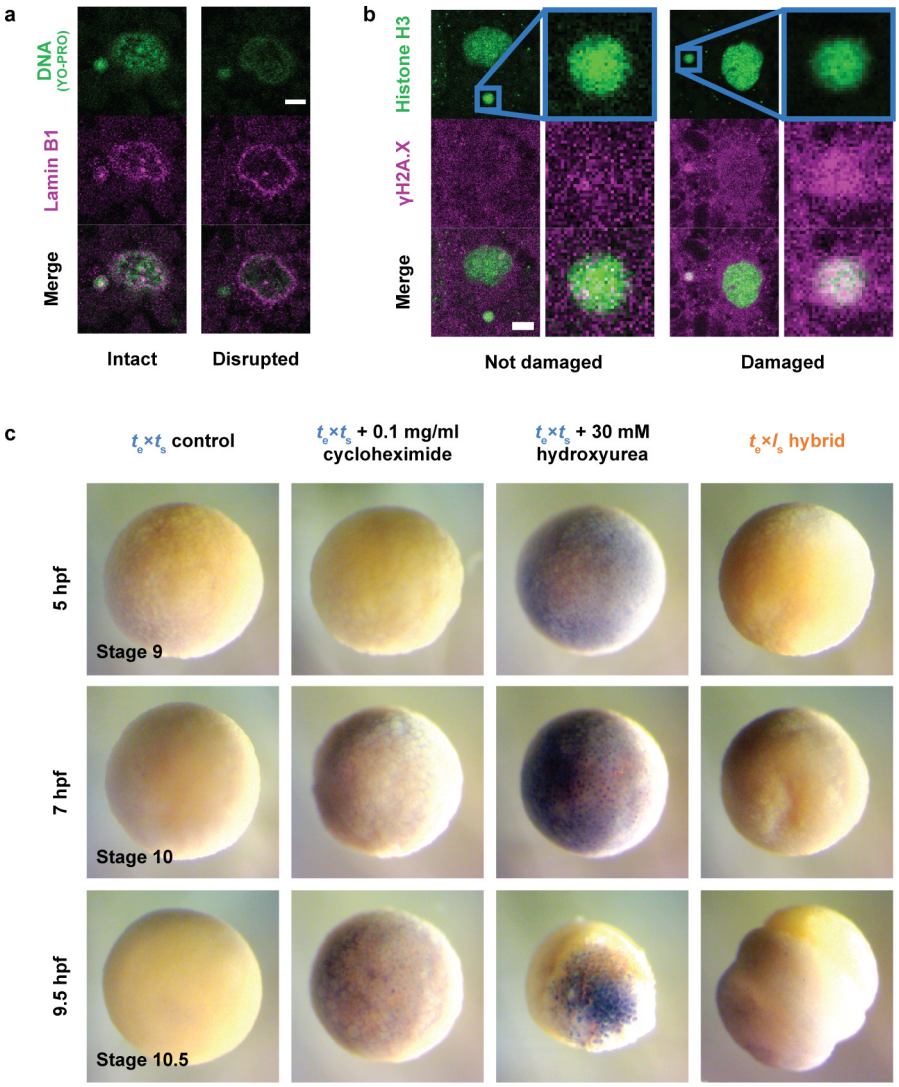

Extended Data Figure 2 | Characterization of micronuclei in $t_e \times l_s$ hybrid embryos and link to embryo death. a, Disrupted micronuclei envelopes in $t_e \times l_s$ hybrid embryos. Whole-mount embryo immunofluorescence was performed in $t_e \times l_s$ hybrid embryos using the YO-PRO DNA dye (top) and anti-Lamin B1 antibody (middle); corresponding channels are shown in green and magenta, respectively. The merged images are shown below. Twenty-five micronuclei within five different embryos were analysed. Intact (left) and disrupted (right) envelopes were observed in all analysed embryos. Scale bar, 10 μm. **b**, DNA damage in $t_e \times l_s$ hybrid embryo micronuclei. Whole-mount embryo immunofluorescence was performed in $t_e \times l_s$ hybrid embryos using anti-histone H3 (top) and anti-γH2A.X (middle) antibodies; corresponding channels are shown in green and magenta, respectively. The merge images are shown below. Twenty-one micronuclei within different six embryos were analysed. Micronuclei with undamaged (left; negative γH2A.X signal) and damaged (right; positive γH2A.X signal) DNA were observed in all analysed embryos. Zoomed images of micronuclei are shown on the right of each image. Scale bar, 10 μm. **c**, TUNEL assay in apoptotic *X. tropicalis* and $t_e \times l_s$ hybrid embryos. *X. tropicalis* (left), *X. tropicalis* treated with cycloheximide (middle left) or hydroxyurea (middle right) as indicated, and $t_e \times l_s$ hybrid (right) embryos were prepared for TUNEL assay 5 h.p.f. (equivalent stage 9; top), 7 h.p.f. (equivalent stage 10; middle), and 9.5 h.p.f. (equivalent stage 10.5; bottom). Identical results were obtained over three different experiments. Representative images are shown and were taken under identical conditions.

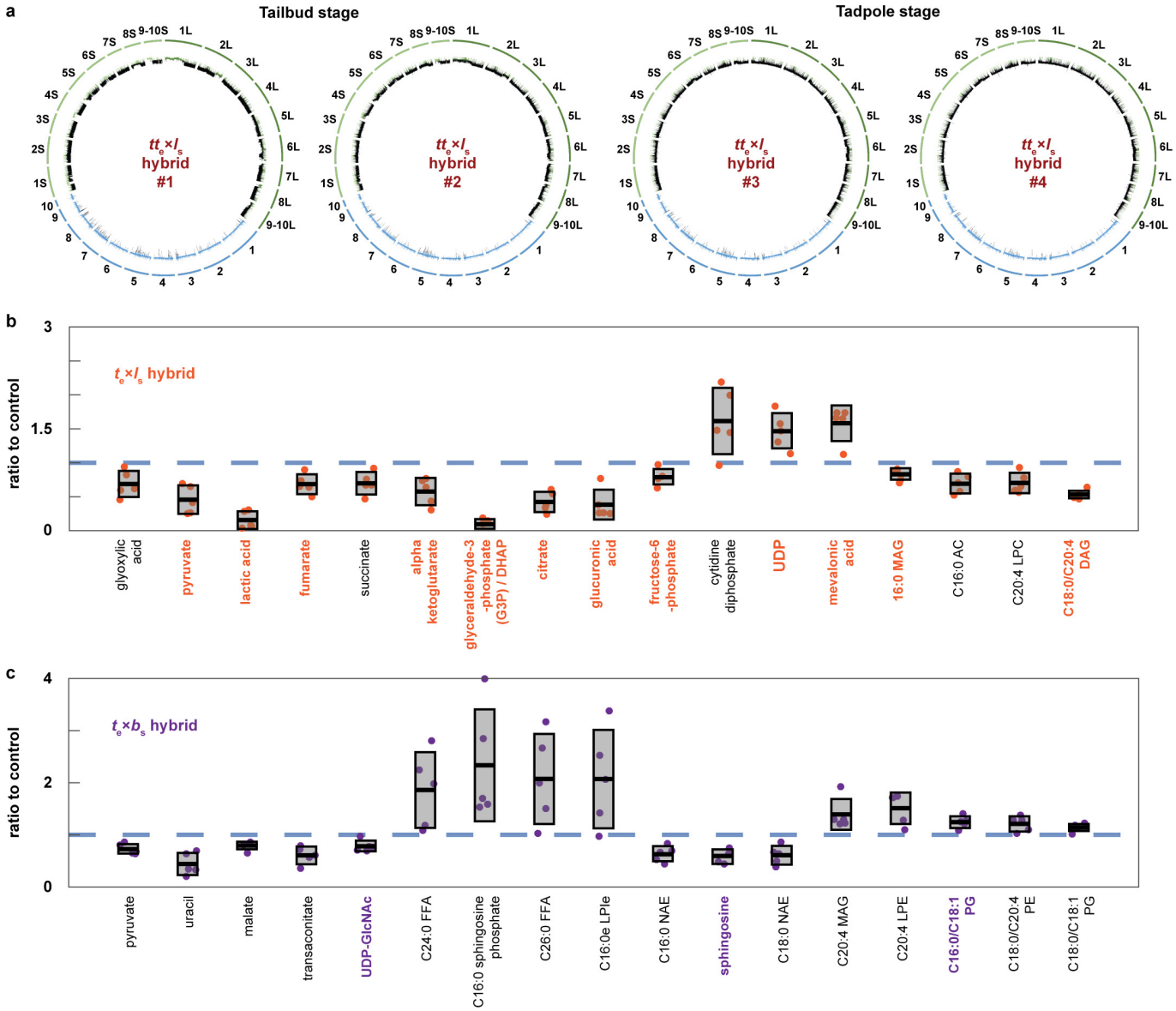

Extended Data Figure 3 | Whole-genome sequencing of $tt_e \times l_s$ rescued embryos and metabolomic profiling of $t_e \times l_s$ and $t_e \times b_s$ hybrid embryos. a, The genomes of 4 $tt_e \times l_s$ rescued embryos were sequenced, aligned, and normalized to the genomes of *X. tropicalis* (blue) and *X. laevis* (green) for which sub-genomes S and L were distinguished (S in light green and L in dark green). Underrepresented regions of the genomes are colour-coded in black. The $tt_e \times l_s$ embryo genomes 1 and 2 were prepared from tailbuds, and 3 and 4 from tadpoles. **b**, Metabolites differentially represented between $t_e \times l_s$ hybrid and *X. tropicalis* embryos 7h.p.f. Among the 179 metabolites detected, 17 were significantly altered in $t_e \times l_s$ hybrid embryos ($P < 0.05$; two-tailed homoscedastic *t*-test; individual *P* values are provided in Fig. 3c source data) and are shown as a ratio to the *X. tropicalis* control (blue dashed line). Levels were obtained from five samples from three independent fertilizations each. Values for the $t_e \times l_s$ hybrid are plotted in orange. The averages are shown as thick lines and the grey boxes correspond to 1 s.d. Ninety-five per cent confidence intervals are, from left to right, 0.69 ± 0.24, 0.46 ± 0.26, 0.16 ± 0.16, 0.68 ± 0.18, 0.70 ± 0.21, 0.58 ± 0.25, 0.10 ± 0.09, 0.42 ± 0.19, 0.38 ± 0.27, 0.79 ± 0.15, 1.61 ± 0.61, 1.47 ± 0.33, 1.58 ± 0.33, 0.83 ± 0.11, 0.71 ± 0.18, 0.70 ± 0.19, and 0.53 ± 0.08. Metabolites with *P* values below the penalized Bonferroni corrected threshold ($n = 12$) are labelled in orange. **c**, Metabolites differentially represented between $t_e \times b_s$ hybrid and *X. tropicalis* embryos 7h.p.f. Among the 241 metabolites detected, 17 were significantly altered in $t_e \times b_s$ hybrid embryos ($P < 0.05$; two-tailed homoscedastic *t*-test; individual *P* values are provided in Fig. 4g source data) and are shown as a ratio to the *X. tropicalis* control (blue dashed line). Levels were obtained from five samples from three independent fertilizations, each. Values for the $t_e \times b_s$ hybrid are plotted in purple. The averages are shown as thick lines and the grey boxes correspond to 1 s.d. Ninety-five per cent confidence intervals are, from left to right, 0.73 ± 0.12, 0.44 ± 0.26, 0.80 ± 0.10, 0.61 ± 0.21, 0.78 ± 0.14, 1.86 ± 0.9, 2.33 ± 1.33, 2.07 ± 1.07, 2.07 ± 1.17, 0.63 ± 0.19, 0.59 ± 0.16 0.61 ± 0.22, 1.39 ± 0.37, 1.51 ± 0.38, 1.24 ± 0.14, 1.21 ± 0.18, and 1.14 ± 0.10. Metabolites with *P* values below the penalized Bonferroni corrected threshold ($n = 3$) are labelled in purple.

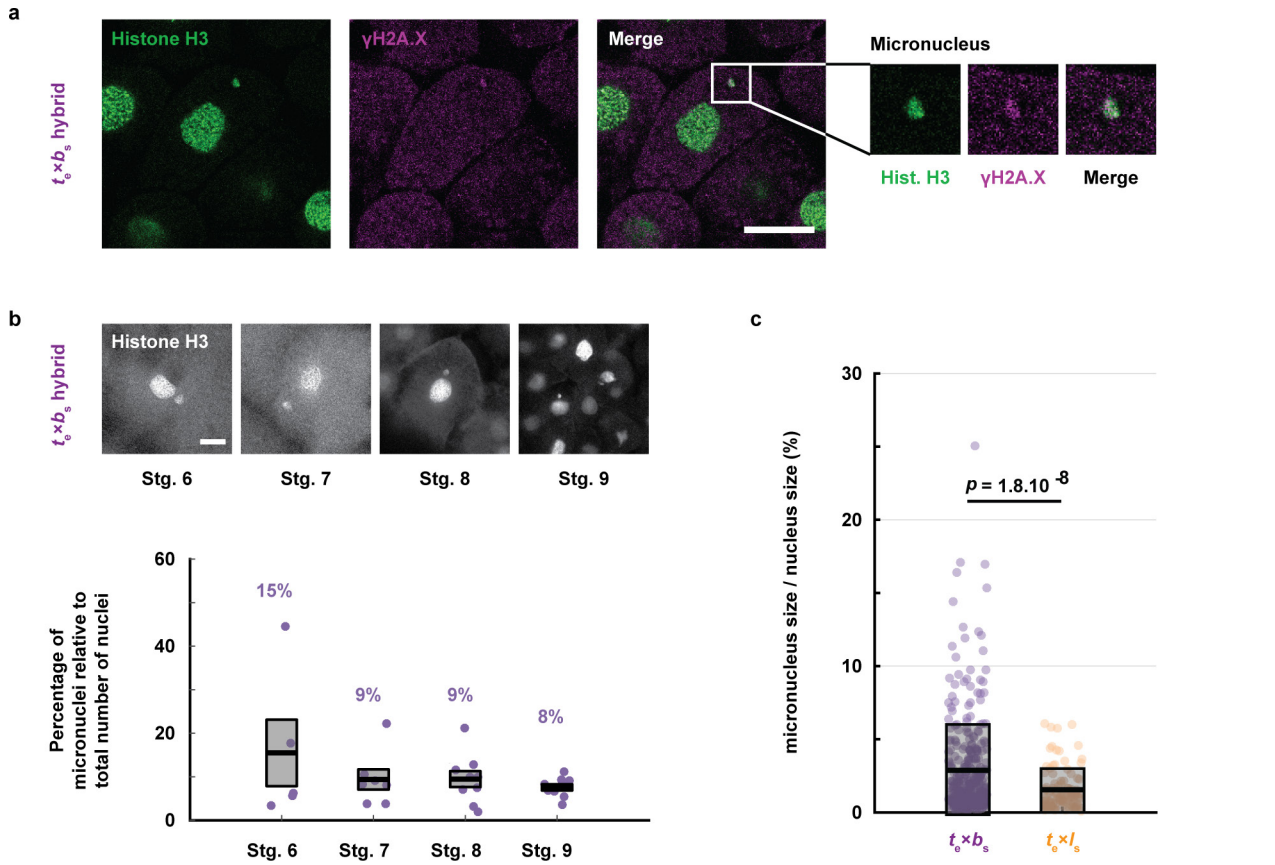

Extended Data Figure 4 | Characterization of micronuclei in $t_e \times b_s$ hybrid embryos. a, DNA damage in $t_e \times b_s$ hybrid embryo micronuclei. Whole-mount embryo immunofluorescence was performed in $t_e \times b_s$ hybrid embryos using anti-histone H3 (left) and anti-γH2A.X (middle) antibodies; corresponding channels are shown in green and magenta, respectively. The merged image is shown on the right. Thirty-four micronuclei within eight different embryos were analysed. Micronuclei with damaged DNA were observed in all analysed embryos. Zoomed images of micronuclei are shown on the right in the same left-to-right order. Scale bar, 20 μm. **b**, Micronuclei in $t_e \times b_s$ hybrid embryos at various developmental stages (top). Whole-mount embryo immunofluorescence was performed in $t_e \times b_s$ hybrid embryos using anti-histone H3 antibody at stages 6, 7, 8, and 9. Scale bar, 20 μm. Quantification of micronuclei in $t_e \times b_s$ hybrid embryos (bottom). The percentage of micronuclei was calculated as the number of micronuclei in the imaged portion of the embryo divided by the total number of nuclei in the same imaged portion. The average percentage for multiple embryos at stage 6 ($n = 5$ $t_e \times b_s$ hybrid embryos (individual dots) with a total of 125 nuclei), stage 7 ($n = 7/153$), stage 8 ($n = 9/731$), and stage 9 ($n = 10/2{,}691$) is shown as a thick line. Grey boxes correspond to 1 s.e.m. Control *X. tropicalis* embryos from the same mothers were analysed but no micronuclei were observed at any stages. **c**, Micronuclei size in $t_e \times b_s$ and $t_e \times l_s$ hybrids. Size is plotted as the ratio between the volumes of the micronucleus and its corresponding nucleus. Each dot represents an individual data point ($n = 329$ micronuclei from 36 $t_e \times b_s$ embryos shown in purple and $n = 100$ from 17 $t_e \times l_s$ embryos shown in orange, from 4 independent experiments). The thick black line indicates the average and the grey box corresponds to 1 s.d. Ninety-five per cent confidence intervals are $2.9 \pm 0.36\%$ for $t_e \times b_s$ and $1.6 \pm 0.28\%$ for $t_e \times l_s$ embryos. Statistical significance was shown using a two-tailed heteroscedastic *t*-test.

Extended Data Table 1 | Embryonic development in *Xenopus* haploids and cybrids generated from *X. tropicalis* irradiated eggs

Embryo	Normal Stage 2† (n)	Regular Stage 9 (%)	Died between 9-13 (%)	Exogastrulae	Normal tailbuds	Abnormal tailbuds	Tadpoles	
							Stunted (%)	Normal (%)
[t_e]× t_s	402 (5)	402 (100)	6 (1)	131 (33)	209 (52)	56 (14)	191 (48)	18 (4)
[t_e]× l_s‡	25 (7)	25 (100)	25 (100)	0 (0)	0 (0)	0 (0)	0 (0)	0 (0)

Symbol *n* indicates the number of different male–female combinations from which results were compiled.
†Unfertilized eggs and embryos that showed an abnormal or incomplete first cleavage were excluded from this analysis.
‡Fertilization efficiency of irradiated *X. tropicalis* eggs with *X. laevis* sperm was very low (~4%).

Extended Data Table 2 | Effects of drug treatments on $t_e \times t_s$ embryos

Drug	Inhibition	Time of addition	Concentration	Phenotype	Product details
Cycloheximide	Protein synthesis	stage 6.5	0.1 mg/ml	Cell cycle arrest at stage 7 followed by apoptosis	C7698 (Sigma-Aldrich)
Hydroxyurea	DNA replication	stage 3	30 mM	Apoptosis at late stage 8	AC151680050 (Thermo Fisher Sc.)
Triptolide	Transcription	stage 2	25 μM	Cell lysis at stage 9	T3652 (Sigma-Aldrich)
Olygomycin	ATP Synthase	stage 2	40 μM	Cell cycle arrest at stage 9	75351 (Sigma-Aldrich)
AP-III-a4	Enolase (including non-glycolytic functions)	stage 2	30 μM	Arrest at stage 7 and followed by cell lysis	19933 (Cayman Chemical)
Iodoacetic acid	Glyceraldehyde-3-P dehydrogenase	stage 2	50 mM	Cell lysis at stage 9	I4386 (Sigma-Aldrich)
CP-91,149	Glycogen phosphorylase	stage 2	270 μM	Cell death at stage 9 from the vegetal side	PZ0104 (Sigma-Aldrich)

X. tropicalis embryos were treated with different drugs at different stages. Phenotypes of effects are listed. When unspecified, apoptosis or lysis initiated at random locations in the embryo.

Extended Data Table 3 | Sub-genome distribution of lost compared with retained DNA in $t_e \times l_s$, $tt_e \times l_s$, and $t_e \times b_s$ hybrids

$t_e \times l_s$ hybrid

Sub genome	Total (bp)	Lost (bp)	Remaining (bp)	Lost (%)	Remaining (%)
X. laevis L	1368982762	237294229	1131688533	17.33	82.67
X. laevis S	1139955720	11850000	1128105720	1.04	98.96
X. tropicalis	1272999256	3452000	1269547256	0.27	99.73

$tt_e \times l_s$ hybrid #1

Sub genome	Total (bp)	Lost (bp)	Remaining (bp)	Lost (%)	Remaining (%)
X. laevis L	1368982762	1084660643	284322119	79.23	20.77
X. laevis S	1139955720	946048452	193907268	82.99	17.01
X. tropicalis	1272999256	5686000	1267313256	0.45	99.55

$tt_e \times l_s$ hybrid #2

Sub genome	Total (bp)	Lost (bp)	Remaining (bp)	Lost (%)	Remaining (%)
X. laevis L	1368982762	1259268028	109714734	91.99	8.01
X. laevis S	1139955720	1003939197	136016523	88.07	11.93
X. tropicalis	1272999256	2964000	1270035256	0.23	99.77

$tt_e \times l_s$ hybrid #3

Sub genome	Total (bp)	Lost (bp)	Remaining (bp)	Lost (%)	Remaining (%)
X. laevis L	1368982762	1360054762	8928000	99.35	0.65
X. laevis S	1139955720	1131571720	8384000	99.26	0.74
X. tropicalis	1272999256	3728000	1269271256	0.29	99.71

$tt_e \times l_s$ hybrid #4

Sub genome	Total (bp)	Lost (bp)	Remaining (bp)	Lost (%)	Remaining (%)
X. laevis L	1368982762	1361764762	7218000	99.47	0.53
X. laevis S	1139955720	1134337720	5618000	99.51	0.49
X. tropicalis	1272999256	3240000	1269759256	0.25	99.75

$t_e \times b_s$ hybrid

Sub genome	Total (bp)	Lost (bp)	Remaining (bp)	Lost (%)	Remaining (%)
X. borealis L	1428994000	108866000	1320128000	7.62%	92.38%
X. borealis S	1201786000	30804000	1170982000	2.56%	97.44%
X. tropicalis	1273010000	11592000	1261418000	0.91%	99.09%

Percentage of lost and remaining DNA for each sub-genome is shown for all hybrid genomes sequenced. Sub-genomes are colour-coded as in Figs 2c and 4e.

Extended Data Table 4 | Overrepresentation test of all or metabolism-only 3L and 4L lost genes

3L and 4L lost genes overrepresentation test	
Analysis Type	PANTHER Overrepresentation Test (release 20170413)
Annotation Version and Release Date	PANTHER version 11.1 Released 2016-10-24
Analyzed List	Client Text Box Input (Xenopus tropicalis)
Reference List	Xenopus tropicalis (all genes in database)
Bonferroni correction	TRUE

PANTHER GO-Slim Biological Process*	**Xenopus tropicalis - REFLIST (18238)**	**Client Text Box Input (843)**	**Client Text Box Input (expected)**	**Client Text Box Input (fold Enrichment)**	**Client Text Box Input (P-value)**	**95% Confidence Interval (binomial test)**
biosynthetic process (GO:0009058)	1295	141	100.05	1.41	8.01E-03	[123.4, ∞]
nitrogen compound metabolic process (GO:0006807)	1738	179	134.27	1.33	1.40E-02	[159.6, ∞]
metabolic process (GO:0008152)	6036	546	466.32	1.17	1.13E-03	[522.4, ∞]

3L and 4L lost metabolism genes overrepresentation test	
Analysis Type	PANTHER Overrepresentation Test (release 20170413)
Annotation Version and Release Date	PANTHER version 11.1 Released 2016-10-24
Analyzed List	Client Text Box Input (Xenopus tropicalis)
Reference List	Xenopus tropicalis (all genes in database)
Bonferroni correction	TRUE

PANTHER GO-Slim Biological Process†	**Xenopus tropicalis - REFLIST (18238)**	**Client Text Box Input (843)**	**Client Text Box Input (expected)**	**Client Text Box Input (fold Enrichment)**	**Client Text Box Input (P-value)**	**95% Confidence Interval (binomial test)**
glycolysis (GO:0006096)	26	6	0.78	7.71	3.71E-02	[2.6, ∞]
rRNA metabolic process (GO:0016072)	104	15	3.11	4.82	2.22E-04	[9.3, ∞]
DNA replication (GO:0006260)	114	16	3.41	4.69	1.38E-04	[10.1, ∞]
tRNA metabolic process (GO:0006399)	104	14	3.11	4.5	1.11E-03	[8.5, ∞]
generation of precursor metabolites and energy (GO:0006091)	185	24	5.54	4.33	9.87E-07	[16.6, ∞]

PANTHER software (http://pantherdb.org/) was used to perform a statistical overrepresentation test on all (top table) or metabolism-only (bottom table) lost genes from chromosomes 3L and 4L.
*Only over-represented processes are shown in the top table.
†Only the top five processes based on fold enrichment are shown in the bottom table.

nature research

Corresponding author(s): Heald, Rebecca

☐ Initial submission ☐ Revised version ☒ Final submission

Life Sciences Reporting Summary

Nature Research wishes to improve the reproducibility of the work that we publish. This form is intended for publication with all accepted life science papers and provides structure for consistency and transparency in reporting. Every life science submission will use this form; some list items might not apply to an individual manuscript, but all fields must be completed for clarity.

For further information on the points included in this form, see Reporting Life Sciences Research. For further information on Nature Research policies, including our data availability policy, see Authors & Referees and the Editorial Policy Checklist.

Experimental design

1. Sample size

Describe how sample size was determined.

Effect sizes were not pre-specified. Sample sizes were sufficient to generate statistically significant differences.

2. Data exclusions

Describe any data exclusions.

No data was excluded

3. Replication

Describe whether the experimental findings were reliably reproduced.

All attempts at replication where successful. All experiments were performed independently at least 3 times.

4. Randomization

Describe how samples/organisms/participants were allocated into experimental groups.

Xenopus frogs were selected randomly from our colony for ovulation and fertilization experiments.

5. Blinding

Describe whether the investigators were blinded to group allocation during data collection and/or analysis.

Investigators were not blinded.

Note: all studies involving animals and/or human research participants must disclose whether blinding and randomization were used.

6. Statistical parameters

For all figures and tables that use statistical methods, confirm that the following items are present in relevant figure legends (or in the Methods section if additional space is needed).

n/a	Confirmed
☐	☒ The exact sample size (*n*) for each experimental group/condition, given as a discrete number and unit of measurement (animals, litters, cultures, etc.)
☐	☒ A description of how samples were collected, noting whether measurements were taken from distinct samples or whether the same sample was measured repeatedly
☐	☒ A statement indicating how many times each experiment was replicated
☐	☒ The statistical test(s) used and whether they are one- or two-sided (note: only common tests should be described solely by name; more complex techniques should be described in the Methods section)
☐	☒ A description of any assumptions or corrections, such as an adjustment for multiple comparisons
☐	☒ The test results (e.g. *P* values) given as exact values whenever possible and with confidence intervals noted
☐	☒ A clear description of statistics including central tendency (e.g. median, mean) and variation (e.g. standard deviation, interquartile range)
☐	☒ Clearly defined error bars

See the web collection on statistics for biologists for further resources and guidance.

Software

Policy information about availability of computer code

7. Software

Describe the software used to analyze the data in this study.	Fiji/ImageJ, version 1.51n MATLAB, version R2016a Microsoft Excel, version 2016 Zeiss Zen Software 2012 SP1, release version 8.1 Micromanager, version 1.4 Imaris, version 8 ToupView, version 3.7.1605 Illumina's bcl2fastq, version 2.17 bwa mem, version 0.7.10 bamUtil, version 1.0.2 BLASTP EnsEMBL, version 80 EdgeR/Bioconductor, version 3.5 PANTHER, version 11.1 R software, version 3.2.2 Limma, version 3.28.10

For manuscripts utilizing custom algorithms or software that are central to the paper but not yet described in the published literature, software must be made available to editors and reviewers upon request. We strongly encourage code deposition in a community repository (e.g. GitHub). *Nature Methods* guidance for providing algorithms and software for publication provides further information on this topic.

Materials and reagents

Policy information about availability of materials

8. Materials availability

Indicate whether there are restrictions on availability of unique materials or if these materials are only available for distribution by a for-profit company.	No unique material was used.

9. Antibodies

Describe the antibodies used and how they were validated for use in the system under study (i.e. assay and species).	No antibodies were made for this study. Antibodies used here are: Mouse anti-beta tubulin (E7; Developmental Studies Hybridoma Bank, Iowa City, IA) Rabbit anti-histone H3 (ab1791; Abcam, Cambridge, MA) Rabbit anti-lamin B1 (ab16048; Abcam, Cambridge, MA) Mouse anti-phospho-histone H2A.X (05-636; EMD Millipore, Merck KGaA, Darmstadt, Germany) Rabbit anti-Ndc80 (validated and provided by Stukenberg lab, University of Virginia) Rabbit anti-CENP-A (validated and provided by Straight lab, Stanford University) Goat anti-mouse or goat anti-rabbit secondary andibodies coupled either to Alexa Fluor 488 or 568 (Invitrogen – Thermo Fisher Scientific, Waltham, MA) Anti-Digoxigenin AP antibody (Roche, Basel, Switzerland) All these antibodies have been previously validated and widely used for studies in Xenopus.

10. Eukaryotic cell lines

a. State the source of each eukaryotic cell line used.	No eukaryotic cell lines were used.
b. Describe the method of cell line authentication used.	Not applicable.
c. Report whether the cell lines were tested for mycoplasma contamination.	Not applicable.
d. If any of the cell lines used are listed in the database of commonly misidentified cell lines maintained by ICLAC, provide a scientific rationale for their use.	Not applicable.

Animals and human research participants

Policy information about studies involving animals; when reporting animal research, follow the ARRIVE guidelines

11. Description of research animals

Provide details on animals and/or animal-derived materials used in the study.

Xenopus laevis (males and females), mature, from 1 to 4 years old
Xenopus tropicalis (males and females), mature, from 6 months to 4 years old
Xenopus borealis (males and females), mature, from 2 to 3 years
Obtained from NASCO and kept in our facility

Policy information about studies involving human research participants

12. Description of human research participants

Describe the covariate-relevant population characteristics of the human research participants.

Human participants were not used in the study.